Cruz Salmeron *et al.*
*Progress in Earth and Planetary Science* (2022) 9:44
https://doi.org/10.1186/s40645-022-00503-5

Progress in Earth and Planetary Science

RESEARCH ARTICLE Open Access

# Characterization of water masses around the southern Ryukyu Islands based on isotopic compositions

Andros Daniel Cruz Salmeron[1], Hideko Takayanagi[1], Shigeyuki Wakaki[2], Tsuyoshi Ishikawa[2], Toshihiro Miyajima[3], Hitomi Wakaki[2], Takuya Itaki[4] and Yasufumi Iryu[1*]

## Abstract

We investigated the water-mass structure on the Okinawa Trough and Pacific sides of the southern Ryukyu Island Arc (Yonaguni, Iriomote, and Ishigaki subareas) using the Nd isotope composition ($^{143}Nd/^{144}Nd$ ratios; expressed as εNd values) of benthic foraminiferal tests in surface sediments, which reflect bottom-water composition, along with hydrogen and oxygen isotope compositions (δD and $\delta^{18}O$ values, respectively) and physical properties (temperature and salinity) of seawater. The Okinawa Trough side has lower εNd values than the Pacific side due to continental/island material inputs characterized by relatively low εNd values. Moreover, within the Okinawa Trough, other processes control the Nd behavior of seawater and primarily affect the Yonaguni and Iriomote subareas, as follows. (1) Surface and subsurface waters are influenced by Taiwanese river discharge combined with temporospatial variations in oceanographic conditions including Kuroshio Current meandering. (2) Intermediate water is characterized by low εNd values (down to − 8.2), possibly attributable to sediment plumes and turbiditic fluxes. (3) The εNd values of bottom water indicate upwelling and vertical mixing, with composition therefore being similar to those of intermediate water. The εNd profiles are better defined on the Pacific side. High εNd values occur in surface and subsurface (< 300 m depth, potential density < 25.0 kg $m^{-3}$) waters, and low values (down to − 7.0) occur in subsurface–core-intermediate water (400–600 m depth, 26–27 kg $m^{-3}$). εNd values increase slightly to − 4.0 below 750 m depth and remain constant down to about 2000 m depth, below which deep water shows a slight decrease in εNd values. Intermediate and bottom/deep waters are distinguished from upper layers by their lower δD and $\delta^{18}O$ values.

**Keywords:** Neodymium isotopes, Hydrogen isotopes, Oxygen isotopes, Kuroshio Current, Okinawa Trough, Ryukyu Islands, Northwestern Pacific

## 1 Introduction

The Kuroshio Current (KC) enters the East China Sea (ECS) through the strait between Taiwan and Yonaguni Jima Island (TY), flows northeastward in the Okinawa Trough (OT) along the Ryukyu Island Arc (RIA), and bifurcates to the southwest of Yaku Shima Island (Fig. 1). The main current changes direction, veering towards the Pacific in the Tokara Strait (TS) area, where the Tokara Gap (TG) lies between Amami Oshima and Yaku Shima islands. The KC is a warm current that transports heat from the tropics to the Ryukyu Islands (the Ryukyus) and the southern half of mainland Japan.

*Correspondence: yasufumi.iryu.d8@tohoku.ac.jp

[1] Institute of Geology and Paleontology, Graduate School of Science, Tohoku University, Sendai, Japan
Full list of author information is available at the end of the article

It has enabled the development of reefs with highly diversified hermatypic coral fauna throughout the Ryukyus, despite their relatively high latitudes within the reef province (Veron 1992) since the opening of the OT and subsequent influx of the KC into the back-arc basin (Iryu et al. 2006). Knowledge of the pathway, strength, and physicochemical properties of the KC is critical for understanding modern oceanographic and climatic conditions in East Asia, and a detailed study of water-mass characteristics around the RIA is expected to contribute to this knowledge.

Neodymium (Nd) is a rare-earth element (REE) with seven naturally occurring isotopes: $^{142}$Nd (27.13% abundance), $^{143}$Nd (12.18%), $^{144}$Nd (23.8%), $^{145}$Nd (8.3%), $^{146}$Nd (17.19%), $^{148}$Nd (5.76%), and $^{150}$Nd (5.64%). Unlike the stable isotope ratios of light elements (e.g., hydrogen, carbon, and oxygen), $^{143}$Nd/$^{144}$Nd ratios, expressed as εNd values (Sect. 3.2), are not affected by isotope fractionation through physical or biogeochemical process, biological cycles, ocean–atmosphere interactions, or seawater temperature changes (Goldstein and Hemming 2003; Lynch-Stieglitz 2003; Klevenz et al. 2008). Because Nd in the oceans is supplied from continents and ocean floors when a water mass is formed, it acquires the εNd values of continent- and ocean-floor-forming rocks. The Nd residence time in oceans (500–1000 yrs) is shorter than the timescales of global oceanic circulation and homogenization (1500–2000 yrs; Tachikawa et al. 2003; Lacan and Jeandel 2005). As a result, the εNd values of the oceans vary with depth and location (Piepgras and Jacobsen 1988; Goldstein and Hemming 2003; Lacan and Jeandel 2005) and are stratified in the water column according to the presence of different water masses (Amakawa et al. 2004b). Therefore, εNd values have been used to identify water masses and reconstruct ocean circulation (Piepgras and Jacobsen 1988; Amakawa et al. 2004b; Wu 2014; Wu et al. 2015a).

Planktic foraminiferal tests record the εNd values of ambient seawater at various depths during their lifespan. After planktic foraminifers die and their tests are transported to the sediment–water interface, the original εNd values are modified to reach isotopic equilibrium with bottom waters over at least 300 yrs (Palmer 1985; Roberts et al. 2012). However, benthic foraminiferal tests comprise calcite precipitated in Nd isotope equilibrium with ambient seawater during both their life and death stages. Because benthic foraminifers also have wide temporospatial distributions, the εNd values of benthic foraminiferal tests have been used to detect variations in the εNd values of bottom water due to water-mass structures (Murray 2013). There is no significant difference in εNd values between a sample of a single benthic foraminiferal species and a sample of multiple foraminiferal species (Haley et al. 2005; Roberts et al. 2012; Wu et al. 2015a); therefore, when single-species samples are limited or unavailable, the εNd values of multi-species samples can be used as a reliable proxy for identifying a water mass and its temporospatial variation (e.g., Palmer 1985; Lynch-Stieglitz and Marchitto 2014).

The ECS is influenced by multiple sources of Nd. The primary source is the Philippine Sea (PS), where εNd values range from −4.4 in deep water to −2.0 in surface–subsurface water (Wu 2014; Behrens et al. 2018). Although in lower proportions, some influence of the South China Sea (SCS) is known to reach the ECS through the TY and the Kerama Gap (KG; Chen 2005; Nakamura et al. 2013). The εNd values in the northeastern SCS vary from −4.5 in deep water to −3.6 in subsurface water, with a surface-water εNd value of −4.5. Many rivers in China flow into the ECS, with the most significant influence being from the Changjiang (εNd = −11.6), Yellow (−13.9 to −9.6), and Yangtze (−14.3 to −8.7) rivers (Meng et al. 2008; Dou et al. 2012). The OT is also influenced by rivers in Taiwan (εNd = −11.1; Lan et al. 2002).

There have been few Nd isotope studies focusing on the OT, and even fewer on the KC. Amakawa et al. (2000) reported εNd values of Kuroshio Surface Water (KSW) at < 5 m depth southeast of Taiwan (εNd = −4.8 at station PA-S-18; 21.83°N, 121.11°E; Fig. 1) and in the western–central OT (−4.9 at station PA-S-19; 26.30°N, 125.54°E; Fig. 1), with these values being lower than those measured to the east of Luzon Strait in the PS (−4.2 at station PA-S-1; 19.54°N, 131.27°E; Fig. 1). A Nd isotope profile at station LM-6/11 (34.16°N, 142°E; Fig. 1) exhibits lower values than those measured to the east of Taiwan (Amakawa et al. 2004b), with εNd values of −5.6 at 5 m depth, −8.7 at 251 m, −6.0 at 503 m, and −5.9 at 1989 m. This SW–NE decrease in εNd values in the KC has been attributed to riverine sediment inputs from the ECS (Amakawa et al. 2004b; Behrens et al. 2018) and transportation of less radiogenic continental Nd (relatively low εNd values) into the central Pacific by the KC (Amakawa et al. 2004a). Dou et al. (2012) identified a post-glacial increase in εNd values during the last deglaciation (from −11.4 at 14 ka to −10.7 at 7 ka) in sediments collected at 766 m water depth on the slope of the ECS shelf, and they interpreted this as reflecting a reduced influence of riverine input from China due to strengthening of the KC. However, no studies have determined the Nd isotope composition in the KC around the RIA at high spatial resolution and over a wide range of depths, with most previous studies focusing on the KC before entry or after exit of the OT.

Stable hydrogen and oxygen isotope compositions, D/H and $^{18}$O/$^{16}$O expressed as δD and $\delta^{18}$O values,

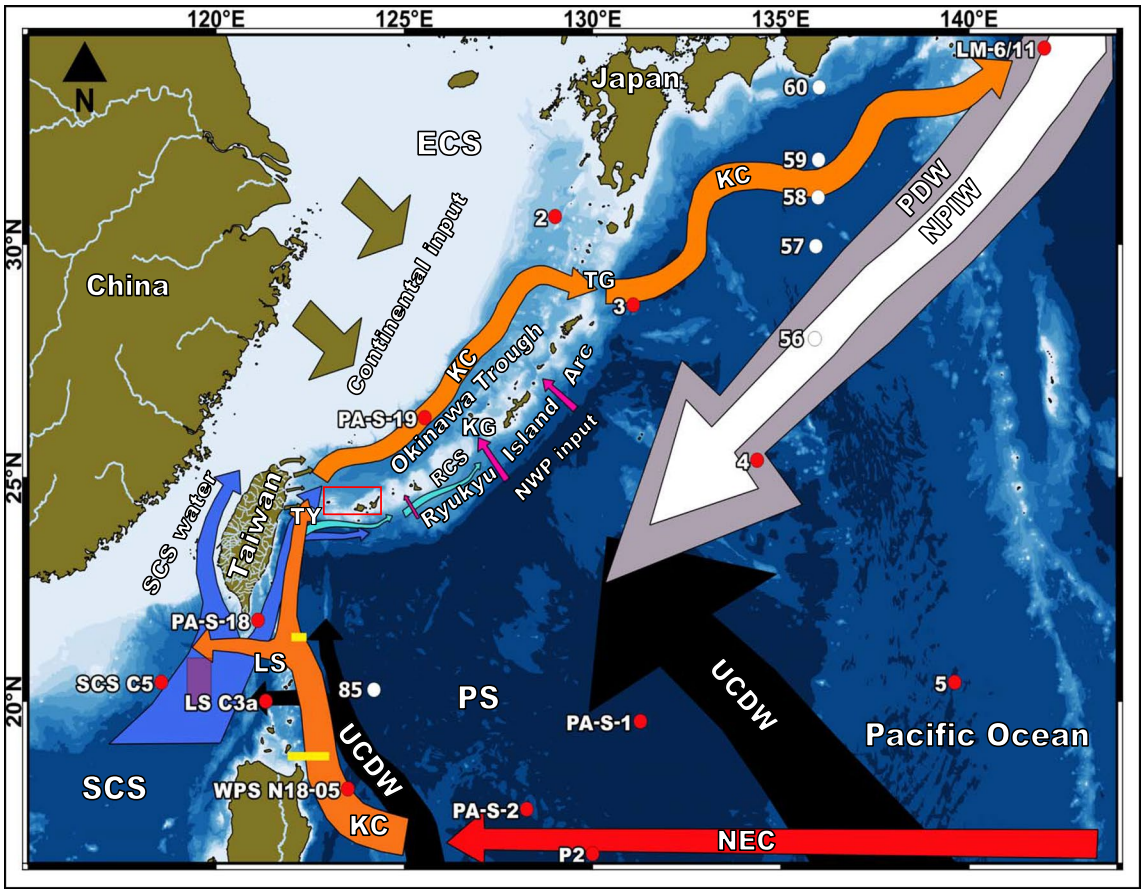


**Fig. 1** Surface and subsurface current systems in the northwestern Pacific Ocean. Red points represent stations from which Nd isotope data have been reported in previous studies: LM-6/11 (Amakawa et al. 2004b); PA-S-1, PA-S-18, and PA-S-19 (Amakawa et al. 2000); 2, 3, 4, and 5 (Behrens et al. 2018); LS C3a, P2, SCS C5, and WPS N18-05 (Wu 2014). Abbreviations: ECS, East China Sea; KC, Kuroshio Current; KG, Kerama Gap; LS, Luzon Strait; NEC, North Equatorial Current; NPIW, North Pacific Intermediate Water; PDW, Pacific Deep Water; PS, Philippine Sea; RCS, Ryukyu Current System; SCS, South China Sea; TY, Strait between Taiwan and Yonaguni Jima Island; TG, Tokara Gap; UCDW, Upper Circumpolar Deep Water. White points represent stations for which δD values were reported by Horibe and Ogura (1968) (Additional file 5: Fig. S3). The horizontal yellow line in the Luzon Strait indicates a transect studied by Mensah et al. (2014)

respectively (Sect. 3.2), provide crucial oceanographic information regarding thermohaline circulation and the formation, mixing, and ventilation of water masses. δD and $\delta^{18}O$ values vary spatially in the oceans depending on advection processes and the mixing of water masses with different isotopic compositions (Xu et al. 2012; Rohling 2013). Transition phases of the hydrological cycle, turbulence fluxes, and Rayleigh distillation affect the δD and $\delta^{18}O$ values of surface water, which change progressively from low to high latitudes. For example, heavier isotopic compositions occur in areas of high evaporation near the Equator, whereas lighter compositions are observed near the poles (Oka and Kawabe 1998; Schmidt et al. 1999; Rohling 2013). The relationships of temperature and salinity to δD and $\delta^{18}O$ values have been broadly used to identify water masses and ocean dynamics (e.g., Horibe and Ogura 1968; Schmidt et al. 1999; Bigg and Rohling, 2000; LeGrande and Schmidt 2006; Sengupta et al. 2013; Wu et al. 2021). Global datasets indicate lower $\delta^{18}O$ values near coastal areas such as the ECS and the PS, which have $\delta^{18}O$ values of −0.1‰ and + 0.1‰, respectively (Bigg and Rohling 2000; LeGrande and Schmidt 2006).

Evaporation and precipitation control salinity–δD and salinity–$\delta^{18}O$ relationships of shallow water distal to continental inputs. When evaporation exceeds precipitation and freshwater discharge, $\delta^{18}O$ and δD values and salinity increase. Conversely, when precipitation and freshwater discharge exceed evaporation, $\delta^{18}O$ and δD values and salinity decrease (Rohling 2013; Sengupta et al. 2013). Furthermore, physical oceanographic processes such as sinking, advection, and upwelling may cause different water masses to have distinct slopes and intercepts

on salinity–δD and salinity–$\delta^{18}O$ cross-plots (Sengupta et al. 2013).

The KC is a source of warm oligotrophic water, so its influx into the OT has been important for the evolution of oceanographic conditions and climate states in Far East Asia. However, past flow paths of the KC and the timing of KC entrance to the OT are poorly constrained. Existing proxies, such as $\delta^{13}C$ and $\delta^{18}O$ values of microfossils, numerical models, and sediment provenance show some discrepancies (e.g., Ujiié et al. 2003; Kao et al. 2006; Dou et al. 2010, 2012; Lee et al. 2013). This study aimed to establish a new proxy of Nd isotope composition that may be used to reconstruct the past water-mass structures of the OT and around the RIA. From a physical oceanography perspective, the OT is a challenging study area due to its complex bathymetry, seasonal-to-interannual variability in seawater physical properties, occurrence of several water masses, and riverine inputs. Therefore, Nd isotopes are expected to provide vital information on the current system and water-mass structure within the OT.

In this study, εNd values were determined by analysis of a small number of modern benthic foraminifers, and the values are directly compared with εNd data from previous studies. This is the first study to delineate variations in εNd values with wide spatial coverage in the KC and related water masses on the OT and Pacific sides of the southern RIA at high spatial resolution, based on εNd, δD, and $\delta^{18}O$ values and physical properties of seawater (e.g., temperature and salinity). The study area is located near the KC entrance to the OT, so it is an ideal site for characterization of the Nd isotope signature of the KC immediately after it interacts with terrigenous materials from the Eurasian continent and Taiwan.

## 2 Study area

### 2.1 Geological settings

The Ryukyus include more than 200 islands and islets to the southwest of mainland Japan, extending from Tanegashima Island (30.73°N, 131°E) in the northeast to Yonaguni Jima Island (24.45°N, 123°E) in the southwest (Fig. 1). The islands are arranged in an arc known as the RIA, an active island arc related to subduction of the Philippine Sea Plate along the Ryukyu Trench beneath the Eurasian Plate. The RIA is bounded by the ECS to the northwest and the Pacific Ocean to the southeast and is geographically divided into three regions (North, Central, and South Ryukyus; Iryu et al. 2006; Arai et al. 2014) by the TG and KG (Fig. 1). The OT is a back-arc basin separating the RIA from the ECS shelf. The study area is located in the western part of the South Ryukyus. The study area on the OT side is divided into three subareas (Fig. 2): Yonaguni (Yonaguni OT), Iriomote (Iriomote OT), and Ishigaki (Ishigaki OT). On the Pacific side, it is also divided into three subareas: Yonaguni (Yonaguni Pacific), Iriomote (Iriomote Pacific), and Ishigaki (Ishigaki Pacific).

The OT has a NE–SW length of ~ 1000 km and a NW–SE width of 200 km. The bathymetry of the trough ranges from shallower depths of ~ 600 m in the north to maximum depths of ~ 2100 m in the Yaeyama and Miyako rifts in the south. Three channels connect the OT with the PS; i.e., the TY, KG, and TG, with maximum water depths of 1700, 2100, and 1500 m and sill depths of 775, ~ 1100, and 700 m, respectively (Arai et al. 2013; Nakamura et al. 2013; Nishizawa et al. 2019).

The opening of the OT and subsequent influx of the KC into the back-arc basin was a key event in the Cenozoic environmental and oceanographic evolution of Far East Asia including the Ryukyus, with the KC being a source of warm oligotrophic water. The initial formation of coral reefs in the Ryukyus is considered to record the influx of the KC into the ECS (i.e., the back-arc side of the RIA). This changed the oceanographic conditions from a "mud sea," represented by siliciclastic deposits of the upper Miocene–lower Pleistocene Shimajiri Group, to a "coral sea," represented by carbonates of the Pleistocene Ryukyu Group that formed in reefs and associated fore-reefs and island shelves (Iryu et al. 2006; Gallagher et al. 2015; Imai et al. 2017).

### 2.2 Oceanographic settings

Here we introduce general aspects of the ocean circulation and water masses in the study area, referring to oceanographic data for the three subareas on the OT and Pacific sides of the RIA (Additional file 1: Tables S1, Additional file 2: Table S2; Fig. 2, Additional file 3: Fig. S1) provided by the Japan Oceanographic Data Center (Japan Oceanographic Data Center, 2021). The JODC temperature and salinity data used in this study were collected from 1 January 1990 to 31 December 2019. Long-term (30 yr) averaging of the data has eliminated short-term variations in temperature and salinity, such as those caused by seasonality, the El Niño–Southern Oscillation, and variability in the KC flow path (Nitani 1975). Therefore, the JODC data are more suitable for characterization of the water masses investigated here than onboard data obtained during the GK19 cruise (Additional file 1: Tables S1, Additional file 2: Table S2). We identified water masses following water-mass classifications of previous studies (Nakamura 1996; Wang and Chen 1998; Qu et al. 1999; Ichikawa and Chaen 2000; Amakawa et al. 2004b; Chen 2005; Talley 2008; Kawabe and Fujio 2010; Talley et al. 2011; Amakawa et al. 2013; Qi et al. 2014; Wu 2014; Yang et al. 2015; Behrens et al. 2018; Zuo et al. 2019). Using the JODC salinity and

temperature data, we calculated potential temperatures and densities and then correlated our results using previous data for the OT and PS (Tables 1 and 2).

#### *2.2.1 Okinawa trough side of the Ryukyu Island Arc*

The North Equatorial Current (NEC) bifurcates into the northward-flowing KC and southward-flowing Mindanao Current to the east of the Philippine coast. The KC enters the OT, flows northeastward along the RIA, and drifts out to the Pacific through the TS. The core of the KC has an average thickness of 500–700 m but reaches depths of up to 1350 m in some areas (Chen 2005; Kubota et al. 2017). Based on physical and chemical properties (e.g., temperature, salinity, nutrients, and pH), three water masses have been identified within the OT in the vertical profile of the KC path: KSW (< 150 m depth), Kuroshio Tropical Water (KTW; 150–300 m depth), and Kuroshio Intermediate Water (KIW; 500–700 m depth; Chen et al. 1995; Wang and Chen 1998; Chen 2005; Mensah et al. 2014). Distinctive KC temperature and salinity fronts exist between the continental shelf region and its offshore region in the OT, with salinity being lower in the former due to freshwater discharge from rivers in China (Oka and Kawabe 1998).

The JODC temperature and salinity data indicate the presence of KSW above ~ 100 m depth, with salinity of 34.47–34.78 and potential density ($\sigma_\theta$) of < 23.0 kg m$^{-3}$. KTW corresponds to the maximum salinity layer at 100–200 m depth, with salinity of 34.81–34.88 and $\sigma_\theta$ of 23.5–24.6 kg m$^{-3}$. Western North Pacific Central Water (WNPCW) is present below the KTW at 250–500 m depth, with salinity of 34.32–34.82 and $\sigma_\theta$ of 25.0–26.4 kg m$^{-3}$ (Table 1, Fig. 4).

Intermediate water resulting from horizontal advection and mixing between North Pacific Intermediate Water (NPIW) and South China Sea Intermediate Water (SCSIW; Nakamura et al. 2013) enters the OT via the KG and TY (Chen 2005; Nakamura et al. 2013;

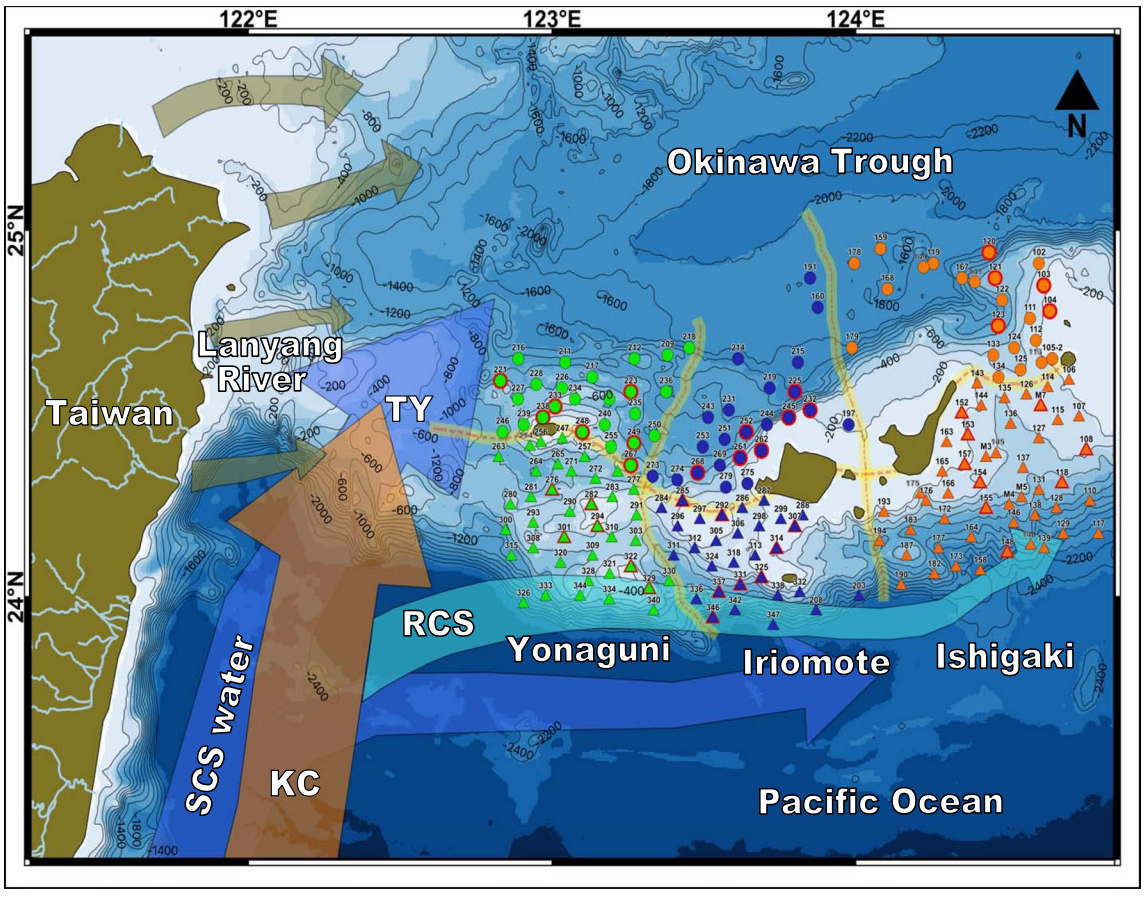


**Fig. 2** Sampling sites in the study area. Circles and triangles represent sites on the Okinawa Trough and Pacific sides of the southern Ryukyu Island Arc, respectively. Green, blue, and orange symbols indicate sites in the Yonaguni, Iriomote, and Ishigaki subareas, respectively. Circles and triangles with red borders indicate sites where sediment samples were collected for Nd isotope analysis. For abbreviations, see Fig. 1

Na et al. 2014). As a result, the salinity of KIW falls to levels between those of NPIW and SCSIW. KIW exists at 500–755 m depth in the OT side, characterized by its low salinity of 34.29–34.36 and $\sigma_\theta$ of 26.5–27.0 kg $m^{-3}$. The intermediate water is more saline by ~ 0.11 on the OT side of the RIA than on the Pacific side, indicating mixing with more saline water within the OT, as for SCSIW (Fig. 3). In the southern OT, the mixing proportions of SCSIW and NPIW are 55% and 45%, respectively (Nakamura et al. 2013). A salinity front separating western high-salinity water from eastern low-salinity water has been detected to the east of Taiwan at 21.45°N near 122.5°E (Chen 2005), suggesting that SCSIW encounters NPIW in this area (Fig. 1). Bottom waters in the OT have salinity of 34.63 and $\sigma_\theta$ of > 27.5 kg $m^{-3}$ (Table 1; Fig. 4).

#### *2.2.2 Pacific side of the RIA*

North Pacific Subtropical Gyre water flows northeastward across the PS on the Pacific side of the RIA, and the subsurface layer has been identified as the Ryukyu Current System (Nakamura et al. 2007; Thoppil et al. 2016). The JODC data indicate that the salinity and $\sigma_\theta$ of surface water (< 83 m depth) are 34.31–34.74 and < 23.00 kg $m^{-3}$ on the Pacific side of the RIA, respectively. However, these values vary seasonally, with salinity being lower in summer and higher in winter (Rudnick et al. 2011). Moreover, the salinity of surface–subsurface water increases in an E–W direction (Chen 2005; Mensah et al. 2014). Salinity maxima correspond to NPTW at 99–216 m depth in the study area (34.67–34.90; $\sigma_\theta$ = 23.5–24.7 kg $m^{-3}$).

Central Water, formed in the subtropics and Equatorial Pacific, overlies North Pacific Intermediate Water (NPIW) and is characterized by a wide range of potential temperature (θ, °C) and salinity. Central Water spreads over the thermocline through advection and diffusion processes over the isopyncals after subduction from the surface mixed layer. For North Pacific Central Water, upper and lower limits correspond to North Pacific Subtropical Mode Water ($\sigma_\theta$ = 25.5 kg $m^{-3}$) and North Pacific Central Mode Water ($\sigma_\theta$ = 26.3 kg $m^{-3}$), respectively (Nakamura, 1996; Talley et al., 2011). Here we refer to this water mass as being WNPCW, identified as having salinity of 34.37–34.82 and $\sigma_\theta$ of 24.9–26.0 kg $m^{-3}$ at 222–476 m depth (Fig. 4).

NPIW has been identified as the minimum-salinity layer in the western PS (Wang and Chen 1998; Qu et al. 1999; Chen 2005; Behrens et al. 2018; Table 2). In the study area, NPIW has salinity of 34.18–34.39 and $\sigma_\theta$ of 26.3–27.2 kg $m^{-3}$.

In the Pacific Ocean, the southern-sourced Lower Circumpolar Deep Water and Upper Circumpolar Deep Water (UCDW) flow in a S–N direction. UCDW upwells at high latitudes in the North Pacific and flows southward as Pacific Deep Water (PDW; Talley et al. 2011). In the PS, PDW can be traced at > 2000 m depth with salinity of 34.6–34.7, θ of 1.6 °C–2.1 °C, and $\sigma_\theta$ of > 27.6 kg $m^{-3}$ (Amakawa et al. 2004b, 2013; Talley 2008; Wu et al. 2015a; Table 2). PDW flows above UCDW to the east of Luzon Strait in the western PS (Wu et al, 2015b; Wan et al. 2018), whereas it is at 1907–2620 m depth in the study area, where salinity is 34.59–34.64 and $\sigma_\theta$ > 27.7 kg $m^{-3}$.

UCDW flows northward in the PS at 3000–3500 m depth (Kawabe and Fujio 2010), encountering the southward-flowing PDW with θ = 1.55 °C and salinity 34.64

**Table 1** Characterization of the water masses in the southern Ryukyu Island Arc. *Only one data available

| | Depth | *T* (°C) | Salinity | $\sigma_\theta$ (kg $m^{-3}$) | δD (‰, average) | $\delta^{18}O$ (‰, average) | εNd |
|---|---|---|---|---|---|---|---|
| *Okinawa Trough side* | | | | | | | |
| Kuroshio Surface Water | < 100 | 23.4–28.2 | 34.47–34.78 | < 23.0 | 4.5* | 0.5* | − 2.2 |
| Kuroshio Tropical Water | 100–200 | 18.6–24.1 | 34.81–34.88 | 23.5–24.6 | 3.6 | 0.4 | − 5.3 to − 5.2 |
| Western North Pacific Central Water | 250–500 | 10.0–18.6 | 34.32–34.82 | 25.0–26.4 | 3.1 | 0.4 | − 6.2 to − 2.8 |
| Kuroshio Intermediate Water | 500–755 | 5.8–9.0 | 34.29–34.36 | 26.5–27.0 | 1.0 | 0.2 | − 5.1 to − 4.8 |
| Deeper Kuroshio Intermediate Water | 755–1900 | 3.6–5.7 | 34.36–34.48 | 27.0–27.5 | 0.4 | 0.0 | − 8.2 to − 4.9 |
| Deep water | 1900–1938 | 2.0 | 34.63 | > 27.5 | – | – | – |
| *Pacific side* | | | | | | | |
| Surface water | < 83 | 24.5–28.6 | 34.31–34.74 | < 23.0 | 3.3 | 0.4 | − 1.7 to − 1.2 |
| North Pacific Tropical Water | 99–216 | 19.3–24.6 | 34.67–34.90 | 23.5–24.7 | 3.4 | 0.4 | − 4.1 to − 1.1 |
| Western North Pacific Central Water | 222–476 | 11.2–18.9 | 34.37–34.82 | 24.9–26.0 | 3.1 | 0.4 | − 5.2 to − 3.4 |
| North Pacific Intermediate Water | 478–863 | 4.9–11.4 | 34.18–34.39 | 26.3–27.2 | 1.3 | 0.1 | − 7.0 to − 3.8 |
| Deeper North Pacific Intermediate Water | 864–1851 | 2.2–4.9 | 34.40–34.61 | 27.2–27.6 | 0.5 | 0.1 | − 4.0 |
| Pacific Deep Water | 1907–2620 | 1.7–2.1 | 34.59–34.64 | > 27.7 | 0.7 | 0.0 | − 5.3 |

**Table 2** Water masses previously reported from the Okinawa Trough and the Pacific Ocean

| Water masses | Depth | Pot. Temp. (°C) | Salinity | $\sigma_\theta$ (kg/m$^3$) | εNd | References |
|---|---|---|---|---|---|---|
| *Pacific Ocean* | | | | | | |
| Surface Water | 0–50 | 26.3–28.71 | > 34.78 | > 22.48 | − 3.5 to − 2.0 | Amakawa et al. (2004b), Wu (2014), Behrens et al. (2018) |
| North Pacific Tropical Water | 61–250 | 18.67–24.50 | 34.75–35.25 | 24.0–24.5 | − 3.1 to − 2.1 | Behrens et al. (2018) |
| Western North Pacific Central Water | 250–400 | 8.5–17.5 | 34.10–34.80 | 25.3–26.5 | − 3.7 to − 3.2 | Nakamura (1996), Talley et al. (2011), Behrens et al. (2018) |
| North Pacific Intermediate Water | 500–700 | 5.13–8.22 | 34.15–34.4 | 26.5–27.2 | − 3.3 to − 2.6 | Wang and Chen (1998), Qu et al. (1999), Chen (2005), Behrens et al. (2018) |
| Pacific Deep Water | > 2000 | 1.55–2.1 | 34.6–34.7 | 27.6 | − 6.0 to − 2.8 | Amakawa et al. (2004b), Talley (2008), Amakawa et al. (2013), Behrens et al. (2018) |
| Upper Circumpolar Deep Water, southern Pacific | 3000–4000 | 1.6–2.1 | 34.6–34.7 | 27.55–28 | − 6.5 to − 4.6 | Talley (2008), Kawabe and Fujio (2010), Amakawa et al. 2013) |
| *South China* | | | | | | |
| South China Sea Surface Water | 0–10 | 24.9–26.3 | 33.9–34.4 | 27.55 | − 4.5 to − 2.9 | Wu (2014), Japan Oceanographic Data Center (2021) |
| South China Sea Intermediate Water | 500–600 | 7.43–8.38 | 34.38–34.43 | 26.25–27.0 | − 4.1 to − 3.6 | Wu (2014), Japan Oceanographic Data Center (2021) |
| *Okinawa Trough* | | | | | | |
| Kuroshio Surface Water | 0–75 | 14–30.2 | 34.2–35.1 | 22.85 | – | Ichikawa and Chaen (2000), Qi et al. (2014), Zuo et al. (2019) |
| Kuroshio Tropical Water | 100–300 | 17–25 | 34.85–35.1 | 23.5–24 | – | Chen (2005), Ichikawa and Chaen (2000),Yang et al. (2015) |
| Kuroshio Intermediate Water | 400–800 | 5–13 | 34.1–34.4 | 26.5–26.77 | – | Chen, (2005), Ichikawa and Chaen (2000), Yang et al. (2015), Zuo et al. (2019) |

(station LM-6/11; Amakawa et al. 2004b) at 27°–30°N (Kawabe et al. 2009). However, it is difficult to separate them within the PS at 1000–2000 m depth because a portion of UCDW upwells (Kawabe and Fujio 2010) and is vertically mixed with PDW. Some authors therefore refer to them as UCDW/PDW (e.g., Behrens et al. 2018).

## 3 Materials and methods

### 3.1 Sampling and sample processing

A total of 189 bottom-water and sediment samples were collected using a K-grab sampler from the area between Ishigaki Jima and Yonaguni Jima islands over a depth range of 68–2620 m during the GK19 cruise of R/V *Kaiyo-maru No. 1* undertaken during June 23–July 22, 2019, by the Geological Survey of Japan of the National Institute of Advanced Industrial Science and Technology (AIST/GSJ; Additional file 1: Tables S1, Additional file 2: Table S2; Fig. 2). Bottom-water samples were collected from ~ 7 m above the seafloor using a Niskin sampler attached to a K-grab sampler. Some physical and chemical properties were measured using a conductivity–temperature–depth (CTD) profiler (CTD 90 M; Sea & Sun Technology GmbH, Germany) attached to the grab sampler. Temperature, salinity, turbidity, pH, and dissolved-oxygen data are presented in Additional file 1: Tables S1 and Additional file 2: Table S2. Surface sediment samples (5–10 cm$^3$; 0–2 cm depth) collected from 42 sites were washed using ultra-pure water and a 63 μm mesh sieve. Particles of > 63 μm size were air-dried at 40 °C for 12 h and sieved using 125 and 250 μm sieves. Samples were divided into three size fractions: 63–125, 125–250, and > 250 μm. Benthic foraminiferal tests (50–70) were handpicked from the > 250 μm fraction under a binocular microscope (Stemi 2000-C; Zeiss, Germany). Although the ages of the samples were not determined, the samples were obtained from 0–2 cm below the seafloor, and previous studies have dated such seafloor sediment at < 1 ka near the study site (Chang et al. 2008; Dou et al. 2012). Figures were processed using QGIS 2.18.19, Ocean Data View (Schlitzer, 2018), and Inkscape version 0.92 (https://inkscape.org/) software. Gridded bathymetric data were taken from the GEBCO Compilation Group (2020), from which isobaths were obtained every 200 m from the digital elevation model using QGIS 2.18.19. Geographical names follow the Gazetteer of Japan 2007 (Geographical Survey Institute of Japan and Japan Coast Guard 2007).

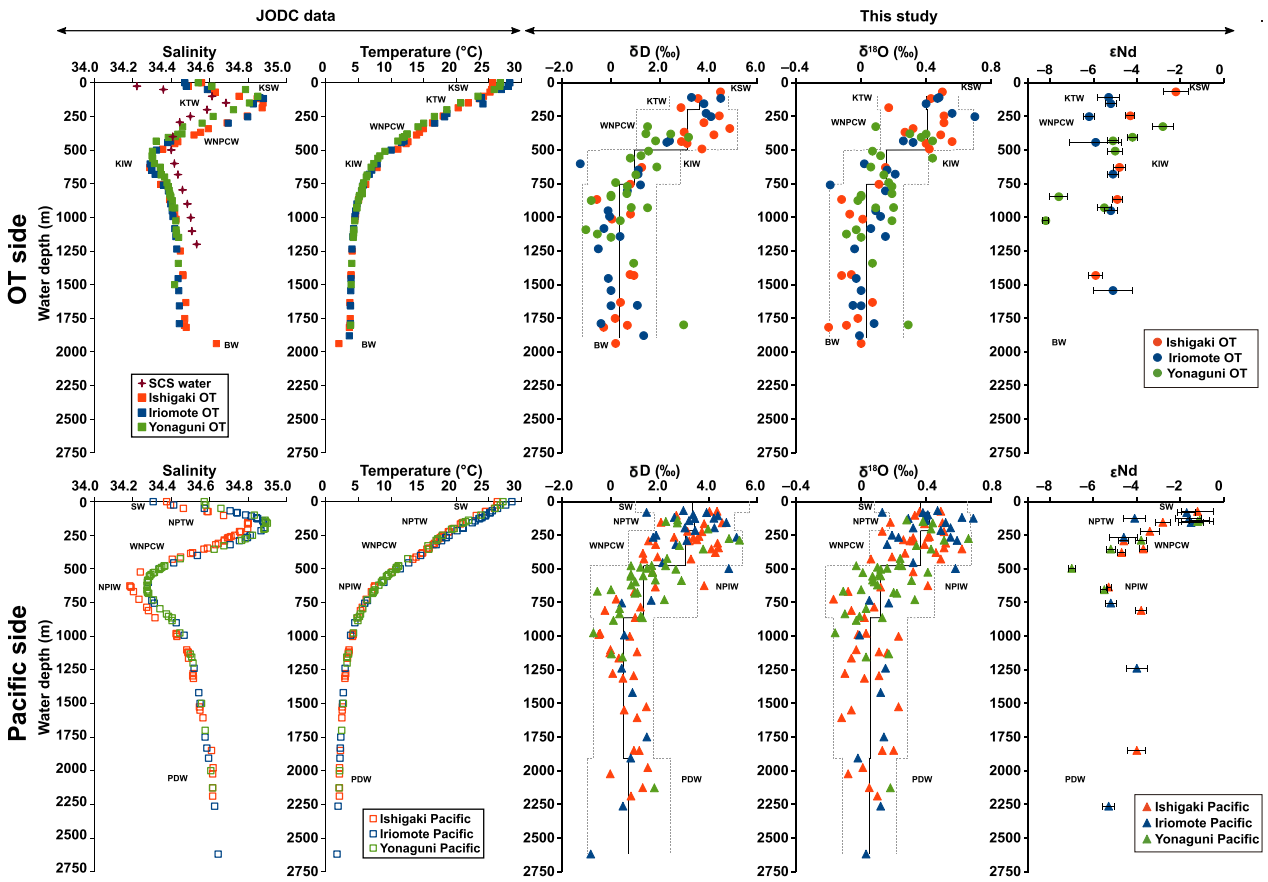


**Fig. 3** Depth profiles of salinity, temperature, and hydrogen (δD), oxygen ($\delta^{18}O$) and neodymium (εNd) isotope compositions for the Okinawa Trough (upper panels) and Pacific (lower panels) sides of the southern Ryukyu Island Arc. The salinity and temperature profiles are based on the data collected from 1 January 1990 to 31 December 2019 (Japan Oceanographic Data Center 2021). Wine-colored symbols in the salinity profile of the Okinawa Trough side indicate salinity measured in the South China Sea water (Japan Oceanographic Data Center 2021). Solid lines in the δD and $\delta^{18}O$ profiles indicate mean δD and $\delta^{18}O$ values in individual water masses. Dotted lines indicate mean ± 2σ ranges. Horizontal bars in the Nd isotope profiles represent analytical errors (2SD). Okinawa Trough side (upper panels): KSW, Kuroshio Surface Water; KTW, Kuroshio Tropical Water; WNPCW, Western North Pacific Central Water; KIW, Kuroshio Intermediate Water; BW, Bottom water. Pacific side (lower panels): SW, surface water; NPTW, North Pacific Tropical Water; WNPCW, Western North Pacific Central Water; NPIW, North Pacific Intermediate Water; PDW, Pacific Deep Water

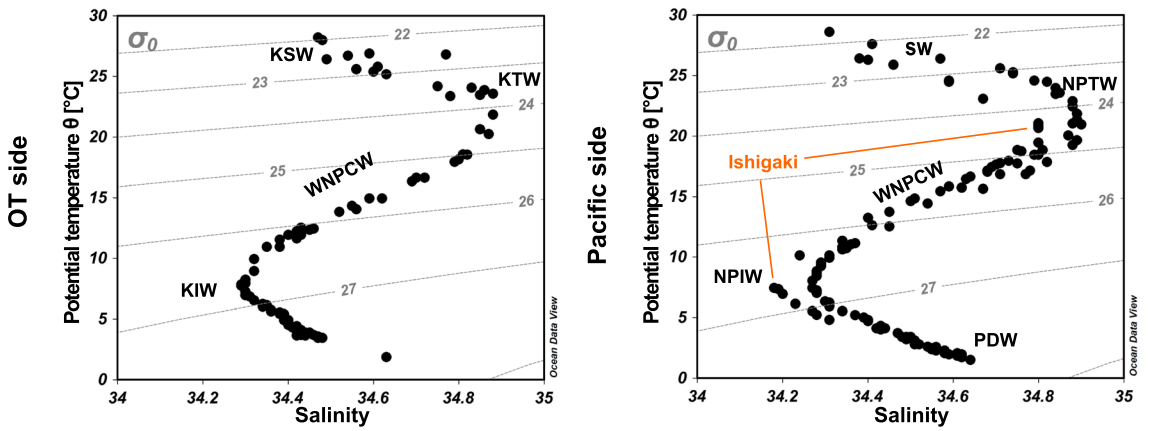


**Fig. 4** Potential temperature–salinity plots for the Okinawa Trough (left panel) and Pacific (right panel) sides of the southern Ryukyu Island Arc. Data from the Japan Oceanographic Data Center (2021)

### 3.2 Sediment sample preparation and Nd isotope analyses

Forty-two sediment samples were selected for Nd isotope analysis. The cleaning of bulk benthic foraminifers followed Lea et al. (2000) and Sagawa et al. (2005). Bulk benthic foraminiferal samples were collected in a 1.5 mL micro-centrifuge tube and decontaminated using a multi-step cleaning procedure, including clay removal using ultrapure water and methanol, reductive cleaning to remove oxidized metal coatings using hydrazine/ammonium citrate, and oxidative cleaning to remove organic matter using $H_2O_2$ buffered by NaOH. The cleaning was undertaken at the Institute of Geology and Paleontology, Graduate School of Science, Tohoku University, Japan.

Nd isotope ($^{143}Nd/^{144}Nd$) analysis of sub-nanogram–nanogram Nd samples followed Wakaki and Ishikawa (2018). The Nd in bulk benthic foraminiferal samples was chemically separated and purified using a three-step extraction and ion-exchange chromatographic procedure. First, Nd was separated from major elements and other REEs using TRU and Ln resins (Eichrom, USA) following a procedure modified from that of Pin and Santos (1997). Sample solutions were first loaded onto Teflon columns filled with 0.2 mL of TRU resin. Major elements were eluted with 4 mL 3 M $HNO_3$, before light REEs (LREEs) were eluted with 2 mL $H_2O$. Eluted LREEs were loaded directly onto a second Teflon column filled with 0.5 mL Ln resin. La, Ce, and Pr were eluted with 3.5 mL 0.2 M HCl, and the Nd fraction with 3 mL 0.2 M HCl. Finally, the separated Nd fraction was loaded onto a third Teflon column filled with 0.1 mL cation-exchange resin (AG50W-X12; Bio-Rad Laboratories, Inc., Japan) for Nd purification. Impurities, remaining cations, and organic materials that may affect Nd ionization during thermal ionization mass spectrometry (TIMS) were eluted with 1.5 mL 2.5 M HCl, and the purified Nd fraction was collected in 2 mL 6 M HCl and evaporated to dryness.

The purified Nd was dissolved in 2.5 µL 3 M $HNO_3$ and loaded onto degassed Re double filaments with 0.8 µL 0.3 M $H_3PO_4$. Nd isotope ratios were determined using TIMS (Triton, Thermo-Finnigan, USA) at the Kochi Core Center, Japan, using the total evaporation normalization (TEN)–TIMS technique, with $Nd^+$ ions used to analyze the Nd isotope composition of a small amount of sample (Wakaki and Ishikawa 2018). The $^{143}Nd/^{144}Nd$ ratio was corrected by internal normalization using the exponential law with an $^{146}Nd/^{144}Nd$ ratio of 0.7219 (O'Nions et al. 1977) to correct for mass discrimination; $^{143}Nd/^{144}Nd$ ratios were corrected for a small systematic bias based on the recommended $^{143}Nd/^{144}Nd$ value of standard JNdi–1 (0.512115; Tanaka et al. 2000). The final analytical error for the normalized $^{143}Nd/^{144}Nd$ ratio, expressed as 2σ (Additional file 1: Tables S1, Additional file 2: Table S2), was estimated by error propagation of the counting errors for $^{143}Nd$, $^{144}Nd$, and $^{146}Nd$ through the normalization equation. Results are expressed in εNd epsilon Nd units.

$$\varepsilon Nd = [(^{143}Nd/^{144}Nd_{sample})/(^{143}Nd/^{144}Nd)_{CHUR} - 1] \times 10^4, \quad (1)$$

where $(^{143}Nd/^{144}Nd)_{CHUR} = 0.512638$ (Jacobsen and Wasserburg 1980).

### 3.3 Water sample preparation and hydrogen and oxygen isotope analyses

Bottom-water samples for H and O isotope analyses were collected at 189 sites at depths of 68–2620 m during the GK19 cruise. Samples were filtered with a 0.45 µm membrane filter and collected in 30 mL glass vials, which were sealed immediately after collection and stored in a cool, dark place.

The hydrogen (D/H) and oxygen ($^{18}O/^{16}O$) isotope ratios of the water samples were determined using cavity ring-down spectroscopy (L2120-I Analyzer; Picarro, USA) at the Atmosphere and Ocean Research Institute, The University of Tokyo, Japan, without chemical preprocessing. Measured H and O isotope ratios were calibrated against an in-house standard and converted into the conventional Vienna standard mean ocean water (V-SMOW) scale (per mil; ‰) based on the following equations:

$$\delta D = [(H/D_{sample})/(H/D)_{standard} - 1] \times 10^3 \quad (2)$$

$$\delta^{18}O = [(^{18}O/^{16}O_{sample})/(^{18}O/^{16}O)_{standard} - 1] \times 10^3. \quad (3)$$

External precision for H–O isotope analyses, based on replicate measurements ($n = 38$) of the in-house standard, was ± 0.61‰ for δD and ± 0.10‰ for $\delta^{18}O$.

Temperature and salinity were measured using the CTD profiler at the bottom-water sampling sites; the pH of the bottom-water samples was measured using a compact pH meter (LAQUAtwin-pH-33; Horiba Scientific, Japan) immediately after samples were collected. The external precision (1σ) of pH values, based on replicate measurements of a standard solution (pH = 7.41), was ± 0.02.

## 4 Results

### 4.1 Neodymium isotopes

The εNd values ranged from − 8.2 to − 2.2 on the OT side of the RIA (Fig. 3). Comparison of εNd profiles in the three subareas shows (1) an eastward increase at < 300 m depth in the Iriomote and Ishigaki OT; (2) the occurrence of a water mass with a wide range of εNd values (− 5.9 to − 2.8) at 300–600 m depth; and (3) relatively constant

εNd values (−5.9 to −4.8) at > 600 m depth, with two highly negative values of −7.6 and −8.2 being recorded in the Yonaguni OT at depths of 848 and 1026 m, respectively.

The εNd values ranged from −7.0 to −1.1 on the Pacific side of the RIA (Fig. 3). The Nd isotope profiles of the three subareas on the Pacific side had similar values and trends from surface to deeper waters, with εNd values of −2.8 to −1.1 at < 157 m depth (with an outlier of −4.1 at 125 m in the Iriomote Pacific). At > 222 m depth, εNd values decreased to −5.5 at 656 m depth, with an outlier of −7.0 at 497 m at Yonaguni Pacific, and increased to −4.0 at 1239 m depth (Fig. 3). A value of −5.3 was recorded at 2264 m depth at the Iriomote Pacific site.

### 4.2 Hydrogen isotopes

On the OT side of the RIA, seawater δD values had similar depth trends for the three subareas (Fig. 3), except at 250–500 m depth in the Ishigaki OT where higher values were recorded. δD values were higher at 117–388 m depth (up to 4.9‰), decreasing steadily to a minimum value of −1.0‰ at 1093 m depth. Although average δD values were almost constant at greater depths, an outlier of > 1.3‰ was recorded at 1800 m depth.

The three subareas on the Pacific side also displayed similar trends, with values of up to 5.3‰ above 380 m depth. δD values decreased to their lowest value of −0.7‰ at 976 m depth, before gradually increasing to 1.8‰ at 2128 m depth. A value of −0.8‰ was recorded at 2620 m depth (Fig. 3).

### 4.3 Oxygen isotopes

On the OT side of the RIA, seawater $\delta^{18}O$ values had similar depth trends in the three subareas (Fig. 3), with higher values of up to 0.7‰ being recorded above 298 m depth. Below this depth, values decreased to a minimum of −0.2‰ at 760 m depth, remaining roughly constant at ~ 0.0‰ at greater depths with an outlier of 0.3‰ at 1800 m. The $\delta^{18}O$ profiles on the Pacific side also had similar trends in the three subareas, with $\delta^{18}O$ values being higher above 285 m depth (up to 0.7‰) and decreasing to −0.2‰ at 726–976 m depth before increasing to 2.0‰ at 1850 m depth (Fig. 3).

## 5 Discussion

### 5.1 Nd isotopes

#### *5.1.1 Surface–subsurface waters*

The εNd values at < 157 m depth ($\sigma_\theta$ < 23.5 kg $m^{-3}$) were −5.3 and −5.2 in the Iriomote OT and −2.2 in the Ishigaki OT; no data were available for the Yonaguni OT. Similarly, low εNd values (−4.3 to −6.2) were recorded at 247–500 m depth ($\sigma_\theta$ = 25.0–26.4 kg $m^{-3}$) in the three subareas on the OT side of the RIA. Surface-water (5 m depth) εNd values of −4.8 and −4.9 have been reported previously southeast of Taiwan (PA-S-18) and west of Okinawa Jima (PA-S-19) (Amakawa et al. 2000; Fig. 1). The εNd values of the KC decrease as it flows to higher latitudes in the OT and then to the southeast of Honshu, as shown by low εNd values of −7.3 to −3.9 (< 200 m depth, station 2; Behrens et al. 2018) and −8.7 to −5.6 (< 455 m depth, station LM-6/11; Amakawa et al. 2004b; Figs. 1 and 5).

When Northwest Pacific waters flow near Taiwan or into the ECS, they are exposed to the influence of sediment and water with low εNd values derived from the Eurasian continent and Taiwan, as indicated by εNd values as low as −6.2 at 0–500 m depth ($\sigma_\theta$ < 26.4 kg $m^{-3}$) on the OT side of the RIA. Possible low-εNd sources include continental rocks of the Eurasian continent (China) and Taiwan, which are enriched in REEs and have strongly negative εNd values of −15.2 to −8.2 (Lan et al. 2002; Li et al. 2013; He et al. 2015). Sediments derived from these rocks are transported to the ocean by numerous rivers, including the Changjiang (εNd = −11.6; Dou et al. 2012), Yellow (−13.9 to −9.6; Meng et al. 2008), and Yangtze (−14.3 to −8.7; Meng et al. 2008) rivers on the Eurasian continent and Taiwan rivers (−11.1; Lan et al. 2002). In contrast, surface water (εNd = −1.7 to −1.2) and NPTW (−3.4 to −1.1) on the Pacific side of the study area retain the Nd isotope signatures of those from the PS, for which similar εNd values (Fig. 5, Table 2) have been reported; e.g., −3.2 to −2.0 (Behrens et al. 2018; Wu 2014).

On the OT side of the RIA, WNPCW is characterized by εNd values of −6.2 to −2.8 at 250–500 m depth ($\sigma_\theta$ = 25.0–26.4 kg $m^{-3}$). On the Pacific side, this water mass has εNd values of −5.2 to −3.4 at 222–476 m depth ($\sigma_\theta$ = 24.9–26.0 kg $m^{-3}$; Fig. 3). In the western PS, North Pacific Subtropical Mode Water at 200–300 m depth ($\sigma_\theta$ = 25.3 kg $m^{-3}$) is characterized by an εNd value of −3.3 (Behrens et al. 2018).

The observation of some high εNd values on the OT side and low values on the Pacific side of the RIA may result from direct interaction with continental inputs in combination with physical processes, as follows.

(1) Ocean circulation is likely to change near continental zones and shelves owing to local topographical effects and physical processes. For example, areas with narrow bathymetry (i.e., the OT) may promote abrupt hydrodynamic behavior that increases horizontal fluxes to values of up to three times vertical fluxes (Huthnance 1995; Lacan and Jeandel 2005; Lambelet et al. 2016).

(2) Westward-moving eddies to the east of Taiwan trigger KC meandering. Differing εNd values between similar locations and depths have been reported in areas

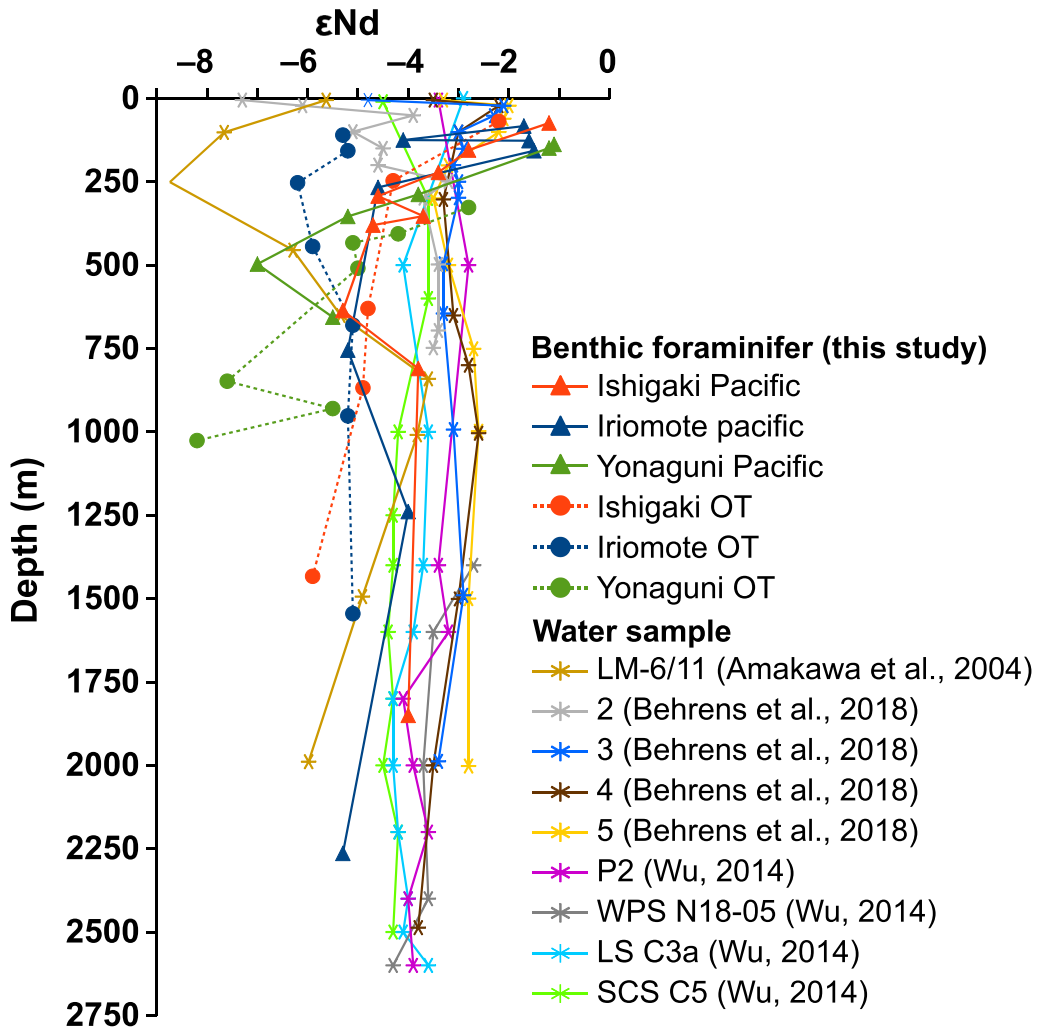


**Fig. 5** εNd profiles for the study area, together with those reported for the northwestern Pacific (Amakawa et al. 2004b; Wu, 2014; Behrens et al. 2018)

under the influence of mesoscale eddies, which play an essential role in vertical and horizontal mixing processes (Grasse et al. 2012). The KC also undergoes periods of high and low transport. At the southeastern tip of Taiwan, a considerable portion of the KC spreads northeastward during low-transport periods, then flows back to the OT between the South Ryukyus (Gawarkiewicz et al. 2011). Drifters released to the east of Taiwan indicate complex spread patterns within the OT and western PS, usually reaching the Pacific side of the study area and, to a lesser extent, as far as Okinawa Jima Island (Gawarkiewicz et al. 2011; Rudnick et al. 2015). Particulates discharged by eastern Taiwan rivers likely follow the same patterns, being deposited on the OT and Pacific sides of the Ryukyus.

(3) Chemical processes controlling the εNd distribution play a significant role in the variable composition of the OT and Pacific sides, as discussed in the following subsections.

#### *5.1.2 Intermediate water*

Intermediate water (mainly of 500–700 m depth; $\sigma_\theta = 26.5–27.0$ kg m$^{-3}$) on both the OT and Pacific sides of the RIA has εNd values mainly in the range of −5.5 to −4.8, at least 1.7 epsilon units lower than those reported for NPIW ($\sigma_\theta$ = 26.67–27.11 kg m$^{-3}$) at similar depths (−3.1 to −2.7; Behrens et al. 2018; −2.8, Wu 2014. Table 2). Although Wu (2014) reported that SCSIW is characterized at similar depths by εNd values ranging from −4.1 (station LS C3a) to −3.6 (station SCS C5; Fig. 1, Table 2), there remains a difference of at least 0.7

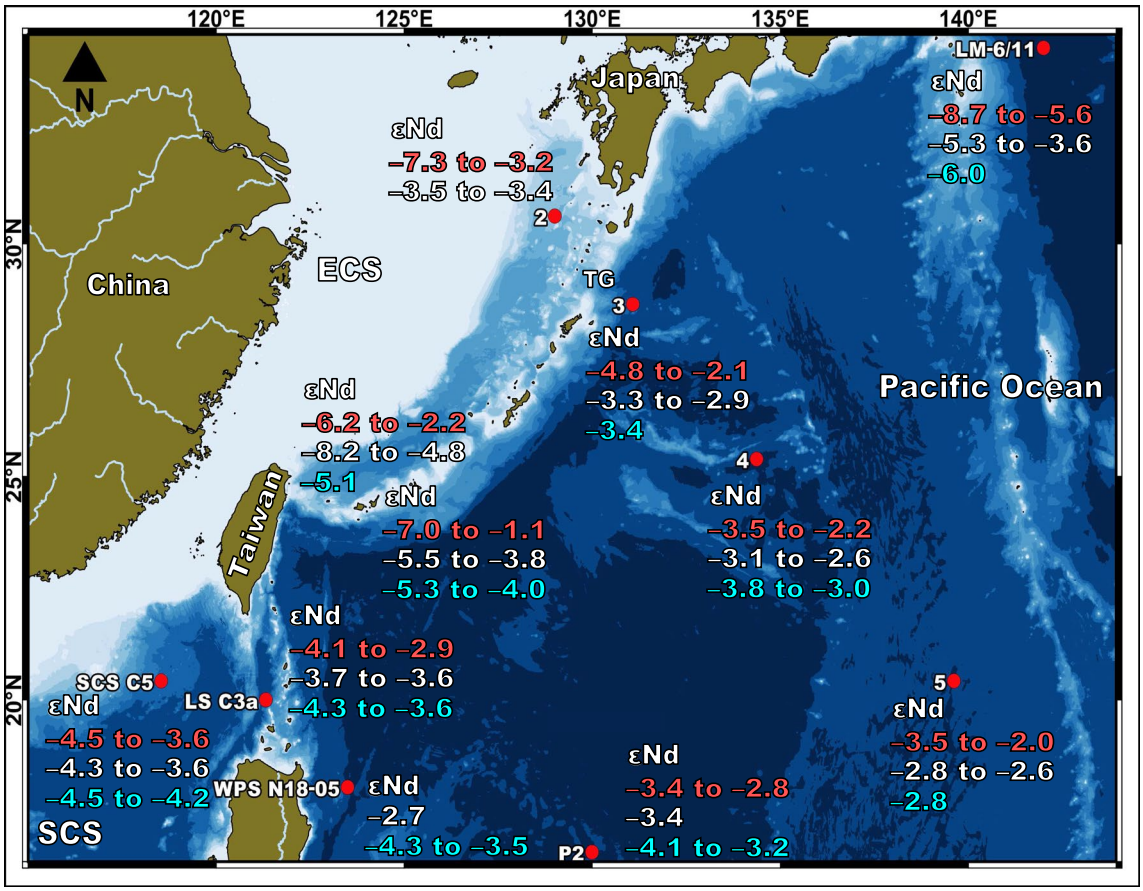


**Fig. 6** εNd values of surface–subsurface (red), intermediate (white), and deep (light blue) waters in the Philippine Sea and the northeastern part of the South China Sea. Data from Amakawa et al. (2004b), Wu (2014) and Behrens et al. (2018)

epsilon units that cannot be explained by the influence of SCSIW around the study area.

The presence of a low-εNd source is indicated by lower εNd values at depths of > 1000 m in the three subareas on the OT side of the RIA (Figs. 3 and 5; e.g., − 8.2 at 1026 m depth in the Yonaguni OT, − 5.1 at 1545 m in the Iriomote OT, and − 5.9 at 1433 m in the Ishigaki OT). OT circulation is controlled mainly by Pacific Ocean water flowing throughout the western margin of the PS and being carried by the KC from subtropical areas, with εNd values of surface–intermediate water in the PS being greater than − 3.7 (Table 2; Behrens et al. 2018). To a lesser extent, SCS surface–subsurface water also flows into the OT (Chen 2005), with εNd values of − 4.5 to − 2.9 (Wu 2014; Fig. 6). Even if SCS water fully controlled circulation within the OT, it could be responsible only for εNd values above − 4.5, which is not the case, so an external source must provide the lower εNd values.

It is apparent that riverine sediments from Taiwan contribute to some extent to low εNd values down to the bottom of the OT. Studies have indicated that up to 60% of the sediment deposited at 1274 m depth at the southwestern corner of the OT is derived from Taiwan (Diekmann et al. 2008; Dou et al. 2016), although from an oceanographic perspective, sediment from Taiwan cannot cross the KC. As the Yonaguni OT is characterized by the occurrence of intermediate water with the lowest εNd values of all water columns investigated in this study, some processes (e.g., turbiditic fluxes) must contribute vertical transport from low-εNd sources to much greater depths. Sediment fluxes in the southern OT increase with depth, suggesting horizontal advection in mid-depth water. Moreover, aluminosilicate plumes identified at depths of 500–700 m may result from resuspended sediments of the Ilan Shelf and Ridge (Hsu et al. 2004).

#### *5.1.3 Deep water*

The εNd values at 1250–1850 m depth ($\sigma_\theta = 27.5$–27.63 kg $m^{-3}$) in the three subareas on the Pacific side of the RIA are about − 4 and lie between those of the western PS (− 4.1 to − 3.2) and SCS (− 4.4 and − 4.3; stations P2 and SCS C5 of Wu (2014), respectively; Fig. 5).

**Table 3** δD and δ18O values of water masses on the Okinawa Trough and Pacific sides of the southern Ryukyu Island Arc

| Water mass | Depth (m) | δD (‰) | | | | $\delta^{18}O$ (‰) | | | |
|---|---|---|---|---|---|---|---|---|---|
| | | Minimum | Average | Maximum | Standard deviation | Minimum | Average | Maximum | Standard deviation |
| *Okinawa Trough side* | | | | | | | | | |
| Kuroshio Surface Water | < 100 | – | 4.5* | – | – | – | 0.5* | – | – |
| Kuroshio Tropical Water | 100– 200 | 2.4 | 3.6 | 4.8 | 0.61 | 0.1 | 0.4 | 0.6 | 0.13 |
| Western North Pacific Central Water | 250– 500 | 1.0 | 3.1 | 5.2 | 1.04 | 0.1 | 0.4 | 0.7 | 0.14 |
| Kuroshio Intermediate Water | 500– 755 | − 0.9 | 1.0 | 2.9 | 0.95 | − 0.1 | 0.2 | 0.4 | 0.13 |
| Deeper Kuroshio Intermediate Water | 755– 1900 | − 1.2 | 0.4 | 1.9 | 0.76 | − 0.2 | 0.0 | 0.3 | 0.11 |
| Bottom water | 1900– 1938 | – | – | – | – | – | – | – | – |
| *Pacific side* | | | | | | | | | |
| Surface water | < 83 | 1.0 | 3.3 | 5.7 | 1.17 | 0.1 | 0.4 | 0.7 | 0.14 |
| North Pacific Tropical Water | 99– 216 | 1.8 | 3.4 | 5.0 | 0.82 | 0.2 | 0.4 | 0.7 | 0.13 |
| Western North Pacific Central Water | 222– 476 | 0.7 | 3.1 | 5.4 | 1.17 | 0.1 | 0.4 | 0.7 | 0.16 |
| North Pacific Intermediate Water | 478– 863 | − 0.9 | 1.3 | 3.5 | 1.10 | − 0.2 | 0.1 | 0.5 | 0.17 |
| Deeper North Pacific Intermediate Water | 864– 1851 | − 0.7 | 0.5 | 1.7 | 0.62 | − 0.2 | 0.1 | 0.3 | 0.11 |
| Pacific Deep Water | 1907– 2620 | − 1.0 | 0.7 | 2.4 | 0.86 | − 0.1 | 0.0 | 0.2 | 0.08 |

*Only one data available

Previous studies have shown that εNd values decrease from the PS toward the SCS, as follows: western PS, εNd = − 2.8 at 1500 m ($\sigma_\theta$ = 27.58 kg $m^{-3}$) at station 5 of Behrens et al. (2018); Luzon Strait, − 3.5 at 1600 m depth at station P2; northeastern SCS, − 3.9 at 1600 m depth at station LS C3a; and − 4.4 at 1600 m depth at station SCS C5 of Wu (2014; Fig. 5). This confirms that SCSIW flows out through the Luzon Strait into the PS at 350–1350 m depth (Wang and Chen 1998). Subsequently, SCSIW encounters NPIW, resulting in KIW having salinity and εNd values between those of SCSIW and NPIW.

Deep waters in the OT are ventilated by intermediate water from the western PS, which enters via the KG at ~ 1100 m depth (Nakamura et al. 2013). However, due to the limited Nd isotope data available for depths > 1500 m ($\sigma_\theta$ > 27.35 kg $m^{-3}$) in the OT, it is difficult to confirm whether its Nd isotope composition is similar to that of upper deep water (~ 2000 m, $\sigma_\theta$ = 27.66 kg $m^{-3}$) on the Pacific side of the RIA. Several factors may explain the low εNd values, as follows.

Our two εNd values for the deepest sites in the OT (− 5.9 at 1433 m, $\sigma_\theta$ = 27.36 kg $m^{-3}$ in the Ishigaki OT; − 5.1 at 1545 m, $\sigma_\theta$ = 27.37 kg $m^{-3}$ in the Iriomote OT) suggest that the upper layer (immediately above 1500 m, $\sigma_\theta$ < 27.35 kg $m^{-3}$) ventilates and imparts a low εNd signature to the lower layer (Fig. 3). It is likely that vertical mixing between intermediate and deeper waters homogenizes the Nd isotope composition below 500 m depth, as indicated by the uniform εNd values (− 5.9 to − 4.8) in the Iriomote and Ishigaki OT. Moreover, salinity and δD and $\delta^{18}O$ values are similar at > 750 m depth ($\sigma_\theta$ > 27.0 kg·$m^{-3}$; Fig. 3). Horibe and Ogura (1968) reported that considerably high δD values characterize not only surface water but also bottom water around the KC path, compared with adjacent open-sea values (Additional file 5: Fig. S3). They suggested that as the KC flows northeastward, the influence of surface and subsurface waters with high δD values reaches deeper waters (e.g., intermediate water had δD values of 4.4‰ at 433 m depth and 3.5‰ at 647 m depth at station 58; Fig. 1). Surface and bottom-water mixing due to a KC-induced flow may reach > 500 m depth. Our results indicate considerably high δD values in deep waters of the study area, with average values of 0.4‰ (σ = 0.8‰) at 1500–1938 m depth on the OT side and 0.7‰ (σ = 0.9‰) at 1907–2620 m depth on the Pacific side (Fig. 3 and Additional file 5: Fig. S3). Therefore, the presence of low εNd values even below the intermediate-water domain must be promoted to some extent by vertical mixing, which decreases with depth as shown by the differences in δD values below 750 m depth (Fig. 3, Table 3).

Another possible explanation of the negative εNd values in the deeper areas is that turbidites, reported at ~ 1400 m depth to the east of Taiwan in the southern OT (Huh et al. 2006), carry sediment with highly negative εNd values to deeper areas. In addition, near continents or marginal seas, the εNd distribution is more complex than that in the open ocean. Therefore, near the continents, the εNd value of a water mass cannot be explained only on the basis of conservative

behavior and water mass mixing/advection, so local sources must be involved (Grasse et al. 2012). Boundary exchange and benthic Nd fluxes may affect the εNd values of seawater in complex ways (Lacan and Jeandel 2005; Abbott et al. 2015). However, as we do not have data to determine whether this process is critical, it is not discussed further here.

Deep-water (2000–3000 m depth, $\sigma_\theta = 27.65$–$27.73$ kg m$^{-3}$) εNd values decrease from east to west in the PS from station 5 ($-3.5$ to $-2.8$) and station 4 ($-3.8$ to $-3.5$) of Behrens et al. (2018) to station P2 ($-4.2$ to $-3.9$) and station WPS N18-05 ($-4.3$ to $-3.6$) of Wu (2014; Figs. 1, 5). Deep water with low εNd signatures of the western PS then flows northeastward to higher latitudes along the western PS margin, as shown by data for the Iriomote Pacific ($-5.3$; this study) and station LM-6/11 ($-6.0$; Amakawa et al. 2004b). Our results indicate that the western PS is more affected by UCDW with low εNd values (i.e., $-6.5$ to $-4.6$; Amakawa et al. 2013) than the eastern PS below the intermediate layer, as shown by lower εNd values in the Iriomote Pacific and Ishigaki Pacific. UCDW flows in a SE–NW direction, bordering Papua New Guinea. About $10 \times 10^6$ m$^3$ s$^{-1}$ (= 10 Sv) of seawater enters the PS via the East and West Caroline basins and the East Mariana Basin. Of the total UCDW influx ($10 \times 10^6$ m$^3$ s$^{-1}$) into the PS, at least $7.5 \times 10^6$ m$^3$ s$^{-1}$ of UCDW does not flow out of the PS, as indicated by the western boundary deep-water flowing to the north at 2650 m depth to the east of Okinawa Jima Island (Kawabe and Fujio 2010). Therefore, the remaining flux must be upwelled, imprinting low εNd signatures on the upper layers by vertical upwelling and mixing.

### 5.2 Hydrogen and oxygen isotopes

The seawater $\delta^{18}$O values and CTD salinity measurements provide snapshot data. The CTD-based salinity ranges are 34.24–34.94 on the OT side and 34.24–34.95 on the Pacific side, whereas the JODC-based salinity (30 yr average) range is 34.29–34.88 on the OT side and 34.18–34.90 on the Pacific side (Additional file 4: Fig. S2). Taking into account salinity–seawater $\delta^{18}$O relationships reported in previous studies (e.g., seawater $\delta^{18}O = 0.31 \times \text{salinity} - 10.3$ in surface water in the South Ryukyus; Abe et al. 2009) and the slight difference between the CTD- and JODC-based salinity, the measured seawater $\delta^{18}$O values are not much different from long-term average seawater $\delta^{18}$O values.

Our δD data are snapshot values rather than long-term data, such as the JODC salinity and temperature data, so they may not necessarily represent average δD values of water masses. However, as the same is true for most of the δD data in previous studies (Benetti et al. 2017; Belem et al. 2019), it is appropriate to use our δD data here in delineating water masses around the RIA. Therefore, the argument based here on δD data is less rigorous than that based on Nd and $\delta^{18}$O data.

On the OT side of the study area, we measured the δD and $\delta^{18}$O values of one sample from KSW in Ishigaki OT. The values were 4.5‰ and 0.5‰ (Additional file 1: Table S1), with average values for KTW of 3.6‰ and 0.4‰, respectively. On the Pacific side of the RIA, surface water had average δD and $\delta^{18}$O values of 3.3‰ and 0.4‰, and NPTW had average values of 3.4‰ and 0.4‰, respectively (Fig. 3, Table 3). These values indicate that high $\delta^{18}$O values characterize the KC, as shown in previous studies (e.g., Horibe and Ogura 1968). Our δD values are similar to those reported previously for NWP waters at low latitudes. For example, Horibe and Ogura (1968) reported δD values of surface water (2.7‰–3.7‰ at < 130 m depth) and tropical water (2.8‰–3.4‰ at 130–174 m) from east of Luzon Island near the KC domain in the western PS (station 85, Fig. 1).

The intermediate-water core on the OT side had average δD and $\delta^{18}$O values of 1.0‰ and 0.2‰, which are lower by ~ 2.1‰ and ~ 0.2‰ than those of WNPCW, respectively (Table 3). On the Pacific side, the values were 1.3‰ and 0.1‰, lower by ~ 1.8‰ and ~ 0.3‰ than WNPCW, respectively. The δD values of the deeper intermediate water (at > 800 m) on the OT side (0.4‰) are almost similar to those on the Pacific side (0.5 ‰), although salinity and potential density data (Sect. 2.2.1) indicate that SCSIW, characterized by lower δD values (e.g., $-0.2$‰–0.1‰ at 448–873 m depth) than NPIW in the western PS (e.g., 0.0‰–0.8‰ at 475–801 m; Horibe and Ogura 1968), enters the OT side. The $\delta^{18}$O values in the study area are consistent with those reported at 600 m depth near Kerama Jima Island (~ 0‰; Takayanagi et al. 2012).

The $\delta^{18}$O value of deep water in the NWP (1499 m depth at 33°N, 146.75°E) is $-0.1$‰ (Bigg and Rohling 2000), which is within the range of values obtained at 876–1500 m depth on the Pacific side of the study area ($-0.1$‰–$-0.2$‰). However, $\delta^{18}$O values are uniformly 0‰ on the OT side of the study area at 755–1938 m depth.

On the OT side of the study area, the δD and $\delta^{18}$O values for KSW (4.5‰ and 0.5‰,) KTW (2.4‰–4.8‰ and 0.1‰–0.6‰), and WNPCW (1.0‰–5.2‰ and 0.1‰–0.7‰) overlap, so the three water masses cannot be distinguished using these isotopes. This is also the case for the Pacific side of the RIA, where the ranges in δD and $\delta^{18}$O values of surface water, NPTW, and WNPCW also overlap.

In contrast, average δD and $\delta^{18}$O values differ between subsurface water ($\delta D \geq 3.1$‰ and $\delta^{18}O \geq 0.4$‰) and intermediate water ($\delta D \leq 1.0$‰ and $\delta^{18}O \leq 0.2$‰) on the OT side of the RIA (Table 3), as is also the case for

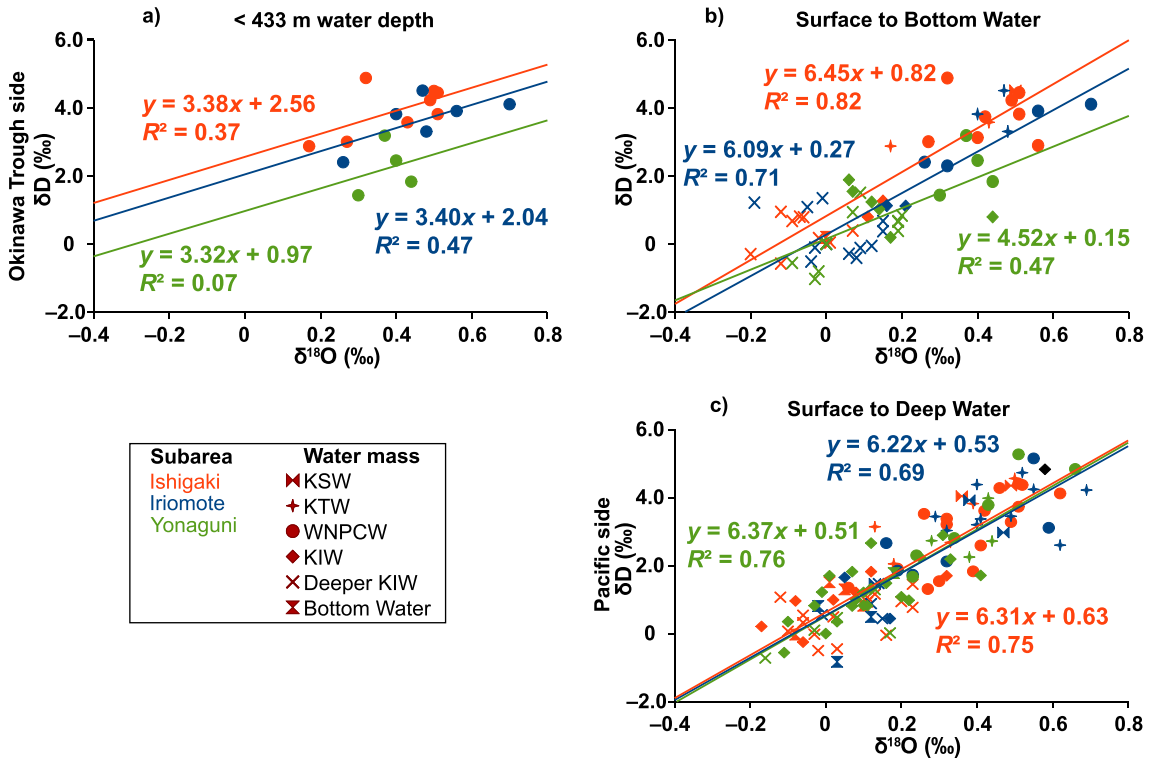


**Fig. 7** $\delta^{18}O$–$\delta D$ cross-plots for seawater on the Okinawa Trough (**a**, **b**) and Pacific (**c**) sides of the study area. **a** Cross-plots for < 433 m depth; **b**, **c** plots for seawater collected from all depths. Outliers for which $\delta^{18}O$ and/or $\delta D$ values are not within the mean ± 2σ range for individual water masses are not shown. For abbreviations, see Fig. 3

subsurface water ($\delta D \geq 3.1‰$ and $\delta^{18}O \geq 0.4‰$) and intermediate water ($\delta D \leq 1.3‰$ and $\delta^{18}O \leq 0.1‰$) on the Pacific side of the RIA (Table 3).

### 5.3 Relationships among temperature, salinity, and hydrogen and oxygen isotopes

The $\delta D$–$\delta^{18}O$ cross-plots for surface–subsurface water (Fig. 7) indicate the influence of runoff near continental areas, with the intercepts representing freshwater inputs (Benetti et al. 2017). The $\delta D$ and $\delta^{18}O$ values of seawater decrease as the influence of freshwater and precipitation increases because freshwater and meteoric water are depleted in D and $^{18}O$. Salinity–$\delta D/\delta^{18}O$ and temperature–$\delta D/\delta^{18}O$ relationships (Additional file 6: Fig. S4) have been used to characterize water masses, delineate water-mass mixing, and identify the influence of precipitation/evaporation on surface waters. The three subareas on the Pacific side of the RIA display similar trends in cross-plots for surface to deep waters (Fig. 7c), with none of the three subareas forming a discrete cluster of values. This reflects a more stable circulation, which could be attributed to the long-distance high-speed KC and the complex fluxes generated. Intermediate water in Ishigaki Pacific (orange rhombuses) subarea is clustered to the left of the Iriomote and Yonaguni subareas, as it is characterized by the lowest salinities (Additional file 6: Fig. S4e). In addition, in Fig. 4, the Ishigaki Pacific corresponds to the low salinity curve. This correspondence is likely to be attributed to the difference in salinities between NPIW and SCSIW. Therefore, the Ishigaki Pacific better retains the physical properties of NPIW, which is represented by a distinctive curve with the lowest salinities at about 600–700 m water depth, between $\sigma_\theta = 26$ and 27 kg m$^{-3}$.

Intermediate water on the OT side of the RIA is more saline by ~ 0.11 than that on the Pacific side, for which there are two possible explanations. First, PDW is more saline than intermediate water, and as it approaches the RIA with decreasing depth, it may mix with the intermediate water before entering the OT. However, this is not plausible, because deep water in the OT is topographically isolated from western PDW (UCDW and North Pacific deep water; Nakamura et al. 2013; Behrens et al. 2018). Although the ventilation process in the OT is not well understood, $\sigma_\theta$ at > 1500 m depth on both the OT and Pacific sides of the RIA ($\sigma_\theta = 27.4$ kg m$^{-3}$) indicates that the deeper intermediate water flowing from the northern PS into the OT via the KG at ~ 1100 m depth

may ventilate as far as the southern OT (at 2000 m depth; Nakamura et al. 2013). The second and more plausible explanation for the higher salinity is that the SCSIW (Wang and Chen 1998; Chen 2005), which is modified KIW becoming more saline in the southern SCS (salinity 34.6; Qu et al. 1999), flows out through the Luzon Strait at 350–1350 m depth (Wang and Chen 1998) with salinity of 34.4–34.6 (Gong et al. 1992; Qu et al. 2000). The mixed water comprising SCSIW (55%; wine-colored symbols in Fig. 3) and NPIW (45%) enters the OT via the TY (Nakamura et al. 2013). A salinity front separating western high-salinity water from eastern low-salinity water has been detected to the east of Taiwan at 21.45°N (Chen 2005), suggesting that SCSIW interacts with NPIW in this area. The KC has a turbulent flux that causes surface and subsurface waters to reach down to 500 m depth (Horibe and Ogura 1968). Bottom-water upwelling has been reported from the southern OT (Nakamura et al. 2013). Therefore, the minimum salinity layer within the OT may increase through vertical mixing with higher salinity of upper and lower layers.

From surface to bottom water, the Ishigaki OT has an intercept of 0.82, Iriomote OT 0.27, and Yonaguni OT 0.15. The very different pattern for Yonaguni OT is caused by the lack of data for surface water, resulting in a slope considerably lower than those of the Iriomote and Ishigaki OT (Fig. 7b). The $\delta^{18}O$–$\delta D$ relationship at < 433 m depth on the OT side indicates that the Ishigaki OT has the highest intercept ($\delta D = 2.56‰$), followed by Iriomote (2.04‰) and Yonaguni OT (0.97‰). This indicates the more significant influence of riverine discharge in the Yonaguni and Iriomote subareas than in the Ishigaki OT (Fig. 7a). Although the proximity of Yonaguni OT to Taiwan inputs is clear, additional processes must control vertical circulation, as shown by the low εNd values and similar salinities and δD and $\delta^{18}O$ values below 750 m depth. On the OT side, temperature and salinity are lower by ~ 1.0 °C–1.5 °C and ~ 0.03–05 in the Yonaguni OT than in the Iriomote OT and Ishigaki OT, respectively. In contrast, the Iriomote OT shows higher salinities at > 250 m depth (Fig. 3). However, Fig. 4 shows similar θ–salinity curves for the three subareas at $\sigma_\theta = 23$–$25$ kg m$^{-3}$. These results suggest that changes in θ and salinity within the three subareas may be related to vertical variations in physical properties (e.g., a vertical shift of the thermocline). Thermocline shifts are likely to be driven by mesoscale eddies (Chen and Chen 2020), which in turn affect KC behavior (e.g., meandering and upwelling) and sea surface height. Areas with sea surface height anomalies are related to eddies, which promote geostrophic circulation (Itoh and Yasuda 2009). The presence of eddies from the east coast to the northeast of Taiwan (Zhang et al. 2001; Gawarkiewicz et al. 2011) may cause vertical shifts in the physical properties of water around the Yonaguni OT.

Another possibility is as follows. The cross-plots indicate that the δD and $\delta^{18}O$ values of intermediate water in the Yonaguni OT overlap with those of the upper and lower layers. Such a trend is not confirmed for the Iriomote and Ishigaki OT subareas (Fig. 7c–f). The interaction of the KC with the topography of the southern OT may promote cross-shelf and downslope transport, enhancing vertical mixing in this area (Huh et al. 2006). Therefore, a different circulation pattern should govern the Yonaguni OT, causing intermediate water to ventilate down to bottom water.

## 6 Conclusions

The water-mass structure was delineated on the OT and Pacific sides of the southern RIA (off Yonaguni Jima, Iriomote Jima, and Ishigaki Jima islands) based on εNd values of benthic foraminifers, δD and $\delta^{18}O$ values, and physical properties (temperature and salinity) of seawater. δD and $\delta^{18}O$ values were determined for seawater collected at 69–1938 m depth on the OT side and 68–2620 m on the Pacific side of the study area. εNd values were determined for benthic foraminifers collected at 69–1545 m depth on the OT side and 74–2264 m on the Pacific side of the study area. The main results of this study are as follows.

1. Riverine sediment discharging into the ECS, including the southwestern OT, is derived mainly from old continental rocks of the Eurasian continent and Taiwan with low εNd values. The low Nd isotope signature is imprinted in water masses flowing within the OT, resulting in a wide range of εNd values of − 8.2 to − 2.2, with slightly lower values than those of the Pacific side for seawater at the same depth.
2. The OT-side circulation is disturbed when the high-speed KC interacts with the complex and narrow bathymetry. As a result, there are overlapping εNd values between different seawater layers. The εNd values on the OT side suggest that additional processes controlling the Nd behavior of seawater occur in individual seawater layers. Surface and subsurface waters are influenced by Taiwanese river discharge associated with temporospatial variations in oceanographic conditions such as KC meandering; intermediate water has the lowest εNd values (as low as − 8.2), possibly resulting from sediment plumes and turbiditic fluxes; bottom water has εNd values similar to those of intermediate water, suggesting active upwelling and vertical mixing.
3. Unlike the OT side, the Pacific side has better-defined εNd profiles, with more pronounced changes

between subsurface–intermediate and intermediate–bottom water boundaries. Surface and subsurface (> 300 m depth) waters are characterized by high εNd values, contrasting with the low values (down to − 7.0) of subsurface–core intermediate water (400–600 m depth). εNd values increase slightly to − 4.0 below 750 m depth, remaining relatively constant to about 2000 m depth, before decreasing slightly below that.

4. On the OT side, δD–$\delta^{18}$O relationships suggests that the Yonaguni, Iriomote, and Ishigaki subareas have different circulation patterns. Furthermore, the surface–subsurface water in the Yonaguni subarea has the lowest δD and $\delta^{18}$O values, attributed to freshwater inputs from Taiwan.
5. δD and $\delta^{18}$O values are similar at depths of 0–500 m on the OT and Pacific sides, indicating intense vertical mixing. In contrast, intermediate and bottom/deep waters are distinguishable from the upper layers by their lower δD and $\delta^{18}$O values.

#### Abbreviations

CTD profiler: Conductivity–temperature–depth profiler; ECS: East China Sea; JODC: Japan Oceanographic Data Center; KC: Kuroshio Current; KG: Kerama Gap; KIW: Kuroshio Intermediate Water; KSW: Kuroshio Surface Water; KTW: Kuroshio Tropical Water; LREE: Light rare-earth element; NEC: North Equatorial Current; NPIW: North Pacific Intermediate Water; NPTW: North Pacific Tropical Water; NWP: Northwest Pacific; OT: Okinawa Trough; TG: Tokara Gap; TS: Tokara Strait; TY: Strait between Taiwan and Yonaguni Jima Island; PDW: Pacific Deep Water; PS: Philippine Sea; REE: Rare-earth element; RIA: Ryukyu Island Arc; SCS: South China Sea; SCSIW: South China Sea Intermediate Water; TIMS: Thermal ionization mass spectrometry; UCDW: Upper Circumpolar Deep Water; WNPCW: Western North Pacific Central Water.

## Supplementary Information

The online version contains supplementary material available at https://doi.org/10.1186/s40645-022-00503-5.

**Additional file 1: Table S1**. Physical properties and isotopic compositions of seawater on the Okinawa Trough side of the southern Ryukyu Island Arc.

**Additional file 2: Table S2**. Physical properties and isotopic compositions of seawater on the Pacific side of the southern Ryukyu Island Arc.

**Additional file 3: Fig. S1**. Sites at which temperature and salinity data during the period from 1 January 1990 to 31 December 2019 were obtained (Japan Oceanographic Data Center, 2021) from the southern Ryukyu Island Arc. Solid and open squares represent sites on the Okinawa Trough and Pacific sides, respectively. Green, blue, and orange symbols indicate sites in the Yonaguni, Iriomote, and Ishigaki subareas, respectively.

**Additional file 4: Fig. S2**. Depth profiles of salinity and temperature for the Okinawa Trough (upper panel) and Pacific (lower panels) sides of the southern Ryukyu Island Arc. The profiles of the three subareas are based on data collected from 1 January 1990 to 31 December 2019 (Japan Oceanographic Data Center 2021). Gray symbols indicate salinity and temperature measured during the GK19 cruise using a conductivity–temperature–depth profiler.

**Additional file 5: Fig. S3**. δD values of deep water below the Kuroshio Current and in the adjacent open sea. Data from Horibe and Ogura (1968).

**Additional file 6: Fig. S4**. Salinity–δ18O/δD and temperature–δ18O/δD cross-plots of seawater on the Okinawa Trough (a–d) and Pacific (e–h) sides of the southern Ryukyu Island Arc. Outliers for which δ18O and/or δD values were not within the mean ± 2σ range for the individual water masses are not shown. For abbreviations, see Fig. 3.

#### Acknowledgements

We thank the Chief Scientist H. Katayama and onboard scientists of the GK19 cruise for their assistance. We thank Captain H. Yabe and crew of the *Kaiyo Maru No. 1* for their support and assistance aboard their vessel. The manuscript was significantly improved by the comments and suggestions of A. Oka (editor) and two anonymous reviewers.

#### Author contributions

ADCS, HT, and YI conceptualized and designed this study. HT, SW, and TI determined Nd isotope composition. HT and TM undertook H and O isotope analyses. HUW identified benthic foraminifers. TI conducted sedimentological analysis of seafloor samples. All authors collaborated in the interpretation of the data and preparation of the manuscript. All authors read and approved the final manuscript.

#### Funding

This work was financially supported by the Japan Society for the Promotion of Science KAKENHI (Grant-in-Aid for Scientific Research) Grant number 19H04251 to HT and Frontier Research in Duo (FRiD) of Tohoku University to Y.I.

#### Availability of data and materials

Please contact the corresponding author regarding data requests.

## Declarations

#### Competing interests

The authors declare that they have no competing interest.

#### Author details

[1]Institute of Geology and Paleontology, Graduate School of Science, Tohoku University, Sendai, Japan. [2]Kochi Institute for Core Sample Research, Japan Agency for Marine-Earth Science and Technology (JAMSTEC), Yokosuka, Japan. [3]Atmosphere and Ocean Research Institute, The University of Tokyo, Kashiwa, Japan. [4]Geological Survey of Japan, AIST, Marine Geology Research Group/Institute of Geology and Geoinformation, Tsukuba, Japan.

Received: 20 October 2021 Accepted: 7 August 2022
Published online: 17 August 2022

#### References

Abbott AN, Haley BA, McManus J (2015) Bottoms up: sedimentary control of the deep North Pacific Ocean's εNd signature. Geology 43:1035–1035. https://doi.org/10.1130/G37114.1

Abe O, Agata S, Morimoto M, Abe M, Yoshimura K, Hiyama T, Yoshida N (2009) A 6.5-year continuous record of sea surface salinity and seawater isotopic composition at Harbour of Ishigaki Island, southwest Japan. Isotopes Environ Health Stud 45:247–258. https://doi.org/10.1080/10256010903083847

Amakawa H, Alibo DS, Nozaki Y (2000) Nd isotopic composition and REE pattern in the surface waters of the eastern Indian Ocean and its adjacent seas. Geochim Cosmochim Acta 64:1715–1727. https://doi.org/10.1016/S0016-7037(00)00333-1

Amakawa H, Alibo DS, Nozaki Y (2004a) Nd concentration and isotopic composition distributions in surface waters of Northwest Pacific Ocean and its adjacent seas. Geochem J 38:493–504. https://doi.org/10.2343/geochemj.38.493

Amakawa H, Nozaki Y, Alibo DS, Zhang J, Fukugawa K, Nagai H (2004b) Neodymium isotopic variations in Northwest Pacific waters. Geochim Cosmochim Acta 68:715–727. https://doi.org/10.1016/S0016-7037(03)00501-5
Amakawa H, Tazoe H, Obata H, Gamo T, Sano Y, Shen CC (2013) Neodymium isotopic composition and concentration in the Southwest Pacific Ocean. Geochem J 47:409–422. https://doi.org/10.2343/geochemj.2.0260
Arai K, Shimoda G, Ikehara K (2013) Marine geological mapping project in the Okinawa area. Geoinformation for the development of submarine mineral resources. Synthesiology 6:162–169. https://doi.org/10.5571/syntheng.6.158
Arai K, Machiyama H, Chiyonobu S, Matsuda H, Sasaki K, Humblet M, Iryu Y (2014) Subsidence of the Miyako-Sone submarine carbonate platform, east of Miyako-jima Island, northwestern Pacific Ocean. Isl Arc 23:1–15. https://doi.org/10.1111/iar.12051
Behrens M, Pahnke K, Schnetger B, Brumsack H (2018) Sources and processes affecting the distribution of dissolved Nd isotopes and concentrations in the West Pacific. Geochim Cosmochim Acta 222:508–534. https://doi.org/10.1016/j.gca.2017.11.008
Belem AL, Caricchio C, Albuquerque ALS, Venancio IM, Zucchi MDR, Dos Santos THR, Alvarez YG (2019) Salinity and stable oxygen isotope relationship in the Southwestern Atlantic: constraints to paleoclimate reconstructions. An Acad Bras Cienc. https://doi.org/10.1590/0001-3765201920180226
Benetti M, Reverdin G, Aloisi G, Sveinbjörnsdóttir Á (2017) Stable isotopes in surface waters of the Atlantic Ocean: Indicators of ocean-atmosphere water fluxes and oceanic mixing processes. J Geophys Res Oceans 122:4723–4742. https://doi.org/10.1002/2017JC012712
Bigg GR, Rohling EJ (2000) An oxygen isotope data set for marine waters. J Geophys Res Oceans 105:8527–8535. https://doi.org/10.1029/2000JC900005
Chang YP, Wang WL, Yokoyama Y, Matsuzaki H, Kawahata H, Chen MT (2008) Millennial-scale Planktic foraminifer faunal variability in the east china sea during the past 40000 years (IMAGES MD012404 from the Okinawa Trough). Terr Atmos Ocean Sci 19:389–401. https://doi.org/10.3319/TAO.2008.19.4.389(IMAGES)
Chen CTA (2005) Tracing tropical and intermediate waters from the South China Sea to the Okinawa Trough and beyond. J Geophys Res 110:C05012. https://doi.org/10.1029/2004JC002494
Chen X, Chen G (2020) Effect of mesoscale eddy on the thermocline depth over the global ocean: deepen and uplift. Ocean Sci Discuss [preprint]. https://doi.org/10.5194/os-2020-64
Chen CTA, Ruo R, Pai SC, Liu CT, Wong GTF (1995) Exchange of water masses between the East China Sea and the Kuroshio off northeastern Taiwan. Cont Shelf Res 25:19–39. https://doi.org/10.1016/0278-4343(93)E0001-O
Diekmann B, Hofmann J, Henrich R, Fütterer DK, Röhl U, Wei KY (2008) Detrital sediment supply in the southern Okinawa Trough and its relation to sea-level and Kuroshio dynamics during the late Quaternary. Mar Geo 255:85–95. https://doi.org/10.1016/j.margeo.2008.08.001
Dou Y, Yang S, Liu Z, Clift PD, Shi X, Yu H, Berne S (2010) Provenance discrimination of siliciclastic sediments in the middle Okinawa Trough since 30 ka: Constraints from rare earth element compositions. Mar Geol 275:212–220. https://doi.org/10.1016/j.margeo.2010.06.002
Dou Y, Yang S, Liu Z, Shi X, Li J, Yu H, Berne S (2012) Sr–Nd isotopic constraints on terrigenous sediment provenances and Kuroshio Current variability in the Okinawa Trough during the late Quaternary. Palaeogeogr Palaeoclimatol Palaeoecol 356–366:38–47. https://doi.org/10.1016/j.palaeo.2012.09.003
Dou Y, Yang S, Shi X, Clift PD, Liu S, Liu J, Li C, Bi L, Zhao Y (2016) Provenance weathering and erosion records in southern Okinawa Trough sediments since 28 ka: Geochemical and Sr–Nd–Pb isotopic evidences. Chem Geol 425:93–109. https://doi.org/10.1016/j.chemgeo.2016.01.029
Gallagher SJ, Kitamura A, Iryu Y, Itaki T, Koizumi I, Hoiles PW (2015) The Pliocene to recent history of the Kuroshio and Tsushima Currents: a multi-proxy approach. Prog Earth Planet Sci 2:17. https://doi.org/10.1186/s40645-015-0045-6
Gawarkiewicz G, Jan S, Lermusiaux PFJ, McClean JL, Centurioni L, Taylor K, Cornuelle B, Duda TF, Wang J, Yang YJ, Sanford T, Lien R-C, Lee C, Lee MA, Leslie W, Haley PJ Jr, Niiler PP, Gopalakrishnan G, Velez-Belchi P, Lee DK, Kim YY (2011) Circulation and intrusions northeast of Taiwan: Chasing and predicting uncertainty in the cold dome. Oceanogr 24:110–121. https://doi.org/10.5670/oceanog.2011.99
GEBCO Compilation Group (2020) GEBCO 2020 Grid. https://doi.org/10.5285/a29c5465-b138-234d-e053-6c86abc040b9. Accessed April 1, 2021
Geographical Survey Institute of Japan and Japan Coast Guard (2007) Gazetteer of Japan. https://www.gsi.go.jp/kihonjohochousa/gazetteer.html. Accessed April 1, 2021
Goldstein SL, Hemming SR (2003) Long-lived isotopic tracers in oceanography, paleoceanography, and ice-sheet dynamics. In: Turekian KK, Holland HD (eds) Treatise on geochemistry, vol 6, 1st edn. Elsevier, Amsterdam, pp 453–489
Gong GC, Liu KK, Liu CT, Pai SC (1992) The chemical hydrography of the South China Sea west of Luzon and a comparison with the West Philippine Sea. Terr Atmos Ocean Sci 3:587–602
Grasse P, Stichel T, Stumpf R, Stramma L, Frank M (2012) The distribution of neodymium isotopes and concentrations in the Eastern Equatorial Pacific: water mass advection versus particle exchange. Earth Planet Sci Let 353–354:198–207
Haley BA, Klinkhammer GP, Mix AC (2005) Revisiting the rare earth elements in foraminiferal tests. Earth Planet Sci Lett 239:79–97. https://doi.org/10.1016/j.epsl.2005.08.014
He M, Zheng H, Clift PD, Tada R, Wu W, Luo C (2015) Geochemistry of fine-grained sediments in the Yangtze River and the implications for provenance and chemical weathering in East Asia. Prog Earth Planet Sci 2:32. https://doi.org/10.1186/s40645-015-0061-6
Horibe Y, Ogura N (1968) Deuterium content as a parameter of water mass in the ocean. J Geophys Res 73:1239–1249. https://doi.org/10.1029/JB073i004p01239
Hsu SC, Lin FJ, Jeng WL, Chung YC, Shaw LM, Hung KW (2004) Observed sediment fluxes in the southwesternmost Okinawa Trough enhanced by episodic events: flood runoff from Taiwan rivers and large earthquakes. Deep-Sea Res Pt I 51:979–997. https://doi.org/10.1016/j.dsr.2004.01.009
Huh CA, Su CC, Wang CH, Lee SY, Lin IT (2006) Sedimentation in the Southern Okinawa Trough-Rates, turbidites and a sediment budget. Mar Geol 231:129–139. https://doi.org/10.1016/j.margeo.2006.05.009
Huthnance JM (1995) Circulation, exchange and water masses at the ocean margin: the role of physical processes at the shelf edge. Prog Oceanog 35:353–431. https://doi.org/10.1016/0079-6611(95)80003-C
Ichikawa H, Chaen M (2000) Seasonal variation of heat and freshwater transports by the Kuroshio in the East China Sea. J Mar Syst 24:119–129. https://doi.org/10.1016/S0924-7963(99)00082-2
Imai R, Sato T, Iryu Y (2017) Calcareous nannofossil assemblages of the upper Miocene to Pliocene Shimajiri Group on Okinawa-jima, Ryukyu Islands, southwestern Japan. J Asian Ear Sci 135:16–24. https://doi.org/10.1016/j.jseaes.2016.12.011
Iryu Y, Matsuda H, Machiyama H, Piller WE, Quinn TM, Mutti M (2006) Introductory perspective on the COREF project. Isl Arc 15:393–406. https://doi.org/10.1111/j.1440-1738.2006.00537.x
Itoh S, Yasuda I (2009) Characteristics of Mesoscale Eddies in the Kuroshio-Oyashio extension region detected from the distribution of the sea surface height anomaly. J Phys Oceano 40:1018–1034. https://doi.org/10.1175/2009JPO4265.1
Jacobsen SB, Wasserburg GJ (1980) Sm–Nd isotopic evolution of chondrites. Earth Planet Sci Lett 50:139–155. https://doi.org/10.1016/0012-821X(80)90125-9
Japan Oceanographic Data Center (JODC) (2021) Serial station data (water samples, STD, CTD, BT) search. https://jdoss1.jodc.go.jp/vpage/scalar.html. Accessed 1 Apr 2021
Kao SJ, Wu CR, Hsin YC, Dai M (2006) Effects of sea level change on the upstream Kuroshio Current through the Okinawa Trough. Geophys Res Lett 33:L16604. https://doi.org/10.1029/2006GL026822
Kawabe M, Fujio S, Yanagimoto D, Takana K (2009) Water masses and currents of deep circulation southwest of the Shatsky Rise in the western North Pacific. Deep-Sea Res Pt I 56:1675–1687. https://doi.org/10.1016/j.dsr.2009.06.003
Kawabe M, Fujio S (2010) Pacific ocean circulation based on observation. J Oceanogr 66:389–403
Klevenz V, Vance D, Schmidt DN, Mezger K (2008) Neodymium isotopes in benthic foraminifera: Core-top systematics and a down-core record from the Neogene south Atlantic. Earth Planet Sci Lett 265:571–587. https://doi.org/10.1016/j.epsl.2007.10.053
Kubota Y, Suzuki N, Kimoto K, Uchida M, Itaki T, Ikehara K, Kim RA, Lee KE (2017) Variation in subsurface water temperature and its link to the Kuroshio

Current in the Okinawa Trough during the last 38.5 kyr. Quat Int 452:1–11. https://doi.org/10.1016/j.quaint.2017.06.021
Lacan F, Jeandel C (2005) Neodymium isotopes as a new tool for quantifying exchange fluxes at the continent-ocean interface. Earth Planet Sci Lett 232:245–257. https://doi.org/10.1016/j.epsl.2005.01.004
Lambelet M, Van de Flierdt T, Crocket K, Rehkämper M, Kreissig K, Coles B, Rijkenberg MJA, Gerringa LJA, De Baar HJW, Steinfeldt R (2016) Neodymium isotopic composition and concentration in the western North Atlantic Ocean: results from the GEOTRACES GA02 section. Geochim Cosmochim Acta 177:1–29. https://doi.org/10.1016/j.gca.2015.12.019
Lan CY, Lee CS, Shen JJS, Lu CY, Mertzman SA, Wu TW (2002) Nd–Sr isotopic composition and geochemistry of sediments from Taiwan and their implications. West Pac Earth Sci 2:205–222
Lea DW, Pak DK, Spero HJ (2000) Climate impact of late Quaternary equatorial Pacific sea surface temperature variations. Science 289:1719–1724. https://doi.org/10.1126/science.289.5485.1719
Lee KE, Lee HJ, Park JH, Chang YP, Ikehara K, Itaki T, Kwon HK (2013) Stability of the Kuroshio path with respect to glacial sea level lowering. Geophys Res Lett 40:392–396. https://doi.org/10.1012/grl.50102
LeGrande AN, Schmidt GA (2006) Global gridded data set of the oxygen isotopic composition in seawater. Geophys Res Lett 33:L12604. https://doi.org/10.1029/2006GL026011
Li CS, Shi XF, Kao SJ, Liu YG, Lyu HH, Zou JJ, Liu SH, Qiao SQ (2013) Rare earth elements in fine-grained sediments of major rivers from the high-standing island of Taiwan. J Asian Earth Sci 69:39–47. https://doi.org/10.1016/j.jseaes.2013.03.001
Lynch-Stieglitz J (2003) Tracers of past ocean circulation. In: Turekian KK, Holland HD (eds) Treatise on geochemistry, vol 6, 1st edn. Elsevier, Amsterdam, pp 435–451
Lynch-Stieglitz J, Marchitto TM (2014) Tracers of past ocean circulation. In: Holland HD, Turekian KK (eds) Treatise on geochemistry, vol 8, 2nd edn. Elsevier, Amsterdam, pp 435–451
Meng X, Liu Y, Shi X, Du D (2008) Nd and Sr isotopic compositions of sediments from the Yellow and Yangtze Rivers: Implications for partitioning tectonic terranes and crust weathering of the Central and Southeast China. Front Earth Sci China 2:418–426. https://doi.org/10.1007/s11707-008-0054-5
Mensah V, Jan S, Chiou MD, Kuo TH, Lien RC (2014) Evolution of the Kuroshio Tropical Water from the Luzon Strait to the east of Taiwan. Deep-Sea Res Pt I 86:68–81. https://doi.org/10.1016/j.dsr.2014.01.005
Murray JW (2013) Living benthic foraminifera: biogeographical distributions and the significance of rare morphospecies. J Micropalaeontol 32:1–58. https://doi.org/10.1144/jmpaleo2012-010
Na H, Wimbush M, Park JH, Nakamura H, Nishina A (2014) Observations of flow variability through the Kerama Gap between the East China Sea and the Northwestern Pacific. J Geophys Res Oceans 119:689–703. https://doi.org/10.1002/2013JC008899
Nakamura H (1996) A pycnostad on the bottom of the ventilated portion in the central subtropical North Pacific: its distribution and formation. J Oceanogr 52:171–188. https://doi.org/10.1007/BF02235668
Nakamura H, Ichikawa H, Nishina A (2007) Numerical study of the dynamics of the Ryukyu Current system. J Geophys Res 112:C04016. https://doi.org/10.1029/2006JC003595
Nakamura H, Nishina A, Liu Z, Tanaka F, Wimbush M, Park J-H (2013) Intermediate and deep water formation in the Okinawa Trough. J Geophys Res 118:6881–6893. https://doi.org/10.1002/2013JC009326
Nishizawa A, Kaneda K, Oikawa M, Horiuchi D, Fujioka Y, Okada C (2019) Seismic structure of rifting in the Okinawa Trough, an active backarc basin of the Ryukyu (Nansei-Shoto) island arc-trench system. Earth Planets Space 71:1–26. https://doi.org/10.1186/s40623-019-0998-6
Nitani H (1975) Variation of the Kuroshio south of Japan. J Oceanogr Soc Jpn 31:154–173. https://doi.org/10.1007/BF02107107
Oka E, Kawabe M (1998) Characteristics of variations of water properties and density structure around the Kuroshio in the East China Sea. J Oceanogr 54:605–617. https://doi.org/10.1007/BF02823281
O'Nions RK, Hamilton PJ, Evensen NM (1977) Variations in $^{143}Nd/^{144}Nd$ and $^{87}Sr/^{86}Sr$ ratios in oceanic basalts. Earth Planet Sci Lett 34:13–22. https://doi.org/10.1016/0012-821X(77)90100-5
Palmer MR (1985) Rare earth elements in foraminifera tests. Earth Planet Sci Lett 73:285–298. https://doi.org/10.1016/0012-821X(85)90077-9
Piepgras DJ, Jacobsen SB (1988) The isotopic composition of neodymium in the North Pacific. Geochim Cosmochim Acta 52:1373–1381. https://doi.org/10.1016/0016-7037(88)90208-6
Pin C, Santos JF (1997) Sequential separation of light rare-earth elements, thorium and uranium by miniaturized extraction chromatography: application to isotopic analyses of silicate rocks. Anal Chim Acta 339:79–89. https://doi.org/10.1016/S0003-2670(96)00499-0
Qi J, Yin B, Zhang Q, Yang D, Xu Z (2014) Analysis of seasonal variation of water masses in East China Sea. Chin J Oceanol Limnol 34(2):958–971. https://doi.org/10.1007/s00343-014-3269-1
Qu T, Mitsudera H, Yamagata T (1999) A climatology of the circulation and water mass distribution near the Philippine Coast. J Phys Oceanogr 29:1488–1505. https://doi.org/10.1175/1520-0485(1999)029%3c1488:ACOTCA%3e2.0.CO;2
Qu T, Mitsudera H, Yamagata T (2000) Intrusion of the North Pacific waters into the South China Sea. J Geophys Res Oceans 105:6415–6424. https://doi.org/10.1029/1999JC900323
Roberts NL, Piotrowski AM, Elderfield H, Eglinton TL, Lomas MW (2012) Rare earth element association with foraminifera. Geochim Cosmochim Acta 94:57–71. https://doi.org/10.1016/j.gca.2012.07.009
Rohling EJ (2013) Oxygen isotope composition of seawater. In: Elias SA (ed) The encyclopedia of quaternary science, vol 2. Elsevier, Amsterdam, pp 915–922
Rudnick DL, Jan S, Centurioni L, Lee CM, Lien RC, Wang J, Lee DK, Tseng RS, Kim YY, Chern CS (2011) Seasonal and mesoscale variability of the Kuroshio near its origin. Oceanogr 24:52–63. https://doi.org/10.5670/oceanog.2011.94
Rudnick DL, Jan S, Lee CM (2015) A new look at circulation in the western North Pacific: Introduction to the special issue. Oceanogr 28:16–23. https://doi.org/10.5670/oceanog.2015.77
Sagawa T, Toyoda K, Oba T (2005) Sea surface temperature record off central Japan since the Last Glacial Maximum using planktonic foraminiferal Mg/Ca thermometry. J Quat Sci 21:63–73. https://doi.org/10.1002/jqs.941
Sengupta S, Parekh A, Chakraborty S, Ravi Kumar K, Bose T (2013) Vertical variation of oxygen isotope in Bay of Bengal and its relationships with water masses. J Geophys Res 118:6411–6424. https://doi.org/10.1002/2013JC008973
Schlitzer R (2018) Ocean Data View. https://odv.awi.de. Accessed April 1, 2021
Schmidt GA, Bigg GR, Rohling EJ (1999) Global seawater oxygen-18 database. http://data.giss.nasa.gov/o18data/. Accessed 24 December 2021
Tachikawa K, Athias V, Jeandel C (2003) Neodymium budget in the modern ocean and paleo-oceanographic implications. J Geophys Res 108(C8):3254. https://doi.org/10.1029/1999JC000285
Takayanagi H, Asami R, Abe O, Kitagawa H, Miyajima T, Iryu Y (2012) Carbon- and oxygen- isotope compositions of a modern deep-water brachiopod *Campagea japonica* collected off Aguni-jima, Central Ryukyu Islands, southwestern Japan. Geochem J 46:7–87. https://doi.org/10.2343/geochemj.1.0153
Talley LD (2008) Freshwater transport estimates and the global overturning circulation: shallow, deep and throughflow components. Prog Oceanogr 78:257–303. https://doi.org/10.1016/j.pocean.2008.05.001
Talley LD, Pickard GE, Emery WJ, Swift JH (2011) Descriptive physical oceanography: an introduction, 6th edn. Elsevier, Amsterdam
Tanaka T, Togashi S, Kamioka H, Amakawa H, Kagami H, Hamamoto T, Yuhara M, Orihashi Y, Yoneda S, Shimizu H, Kamimaru T, Takahashi K, Yonagi T, Nakano T, Fujimaki H, Shinjo R, Asahara Y, Tanimizu M, Dragusanu C (2000) JNdi-1: a neodymium isotopic reference in consistency with LaJolla neodymium. Chem Geol 168:279–281. https://doi.org/10.1016/S0009-2541(00)00198-4
Thoppil PG, Metzger EJ, Hurlburt HE, Smedstad OM, Ichikawa H (2016) The current system east of the Ryukyu Island as revealed by a global ocean reanalysis. Prog Oceanogr 141:239–258. https://doi.org/10.1016/j.pocean.2015.12.013
Ujiié Y, Ujiié H, Taira A, Nakamura T, Oguri K (2003) Spatial and temporal variability of surface water in the Kuroshio source region, Pacific Ocean, over the past 21,000 years: evidence from planktonic foraminifera. Mar Micropaleontol 49:335–364. https://doi.org/10.1016/S0377-8398(03)00062-8
Veron JEN (1992) Conservation of biodiversity: a critical time for the hermatypic corals of Japan. Coral Reefs 11:13–21. https://doi.org/10.1007/BF00291930

Wakaki S, Ishikawa T (2018) Isotope analysis of nanogram to sub-nanogram sized Nd samples by total evaporation normalization thermal ionization mass spectrometry. Int J Mass Spectrom 424:40–48. https://doi.org/10.1016/j.ijms.2017.11.014

Wan S, Jian Z, Dang H (2018) Deep hydrography of the South China Sea and deep water circulation in the Pacific since the Last Glacial Maximum. Geochem Geophys Geosyst 19:1447–1463. https://doi.org/10.1029/2017GC007377

Wang SL, Chen CTA (1998) Bottom water at the center of the north East China Sea in summer: Remnant winter water. Cont Shelf Res 18:1573–1580. https://doi.org/10.1016/S0278-4343(98)00037-5

Wu Q (2014) New insights into the current- and past hydrology of the north-western subtropical Pacific Ocean over the past 25 kyr, based on investigations of the Nd isotopic composition of seawater and deep-sea sediments from the northern South China Sea. Doctoral dissertation, Université Paris Sud-Paris XI

Wu Q, Colin C, Liu Z, Douville E, Dubois-Dauphin Q, Frank N (2015a) New insights into hydrological exchange between the South China Sea and the Western Pacific Ocean based on the Nd isotopic composition of seawater. Deep-Sea Res Pt II 122:25–40. https://doi.org/10.1016/j.dsr2.2015.11.005

Wu Q, Colin C, Liu Z, Thil F, Dubois-Dauphin Q, Frank N, Tachikawa K, Bordier L, Douville E (2015b) Neodymium isotopic composition in foraminifera and authigenic phases of the South China Sea sediments: Implications for the hydrology of the North Pacific Ocean over the past 25 kyr. Geochem Geophys Geosyst 16:3883–3904. https://doi.org/10.1002/2015GC005871

Wu J, Lao Q, Chen F, Huang C, Zhang S, Wang C, Zhou F, Chen C, Zhou X, Lu X (2021) Water mass processes between the South China Sea and the Western Pacific through the Luzon Strait: insights from hydrogen and oxygen isotopes. J Geophys Res Oceans 126:e2021JC017484. https://doi.org/10.1029/2021JC017484

Xu X, Butzin M, Lohmann G (2012) Water isotope variations in the global ocean model MPI-OM. Geosci Model Dev 5:809–818. https://doi.org/10.5194/gmd-5-809-2012

Yang YJ, Jan S, Chang MH, Wang J, Mensah V, Kuo TH, Tsai CJ, Lee CY, Andres M, Centurioni LR, Tseng YH, Liang WD, Lai JW (2015) Mean structure and fluctuations of the Kuroshio East of Taiwan from in situ and remote observations. Oceanography 28:74–83

Zhang DX, Lee TN, Johns WE, Liu CT, Zantopp R (2001) The Kuroshio east of Taiwan: Modes of variability and relationship to interior ocean mesoscale eddies. J Phys Oceanogr 31:1054–1074. https://doi.org/10.1175/1520-0485(2001)031%3c1054:TKEOTM%3e2.0.CO;2

Zuo J, Song J, Yuan H, Li X, Li N, Duan L (2019) Impact of Kuroshio on the dissolved oxygen in the East China Sea region. J Ocean Limnol 37:513–524. https://doi.org/10.1007/s00343-019-7389-5

## Publisher's Note